UMN-TH-1735/99
TPI-MINN-98/30
astro-ph/9901231
January 1999

PRIMORDIAL BIG BANG NUCLEOSYNTHESIS

K.A. OLIVE
School of Physics and Astronomy, Theoretical Physics Institute
University of Minnesota
Minneapolis MN 55455 USA

Abstract. Big Bang Nucleosynthesis is the theory of the production of the light element isotopes of D, ^{3}He, ^{4}He, and ^{7}Li. After a brief review of the essential elements of the standard Big Bang model at a temperature of about 1 MeV, the theoretical input and predictions of BBN are discussed. The theory is tested by the observational determinations of the light element abundances and the current status of these observations is reviewed. Concordance of standard model and the related observations is found over a limited range of the baryon-to-photon ratio, the single true parameter of the standard model. Implications of BBN on chemical evolution, dark matter and constraints on particle properties will be also discussed.

1. Introduction

Big Bang Nucleosynthesis (BBN) is the theory explaining the origins of the light elements D,^{3}He, ^{4}He, and ^{7}Li and their primordial abundances. The theoretical framework for BBN is quite simple. It is based on Friedmann-Lemaitre-Robertson-Walker cosmology [1] and a network of nuclear reactions. We can further specify that the standard BBN model refers to homogeneous nucleosynthesis in the context of a FLRW Universe with an electroweak standard model particle content, which for the purposes of BBN really amounts to assuming the existence of three nearly massless and nearly stable neutrinos. The predictions of BBN for the abundances of the light elements are determined by running a code which incorporates the nuclear network in a thermal (and cooling due to the expansion of the Universe) bath. These predictions are then be compared with the observational determinations of the abundances.

Summary of Lectures given at the Advanced School on Cosmology and Particle Physics, Peniscola, Spain, June 1998 and at the Theoretical and Observational Cosmology Summer School , Cargese, Corsica, France, August 1998.

In contrast to the theoretical side of BBN, the status of the observational data has changed significantly in the last several years. There is more data on ^{4}He and ^{7}Li, and data on D and ^{3}He that was simply non-existent several years ago. For the most part, the inferred abundances of ^{4}He and ^{7}Li have remained relatively fixed, giving us a higher degree of confidence in the assumed primordial abundances of these isotopes as is reflected in their observational uncertainties. Indeed, the abundances of ^{4}He and ^{7}Li alone are sufficient to probe and test the theory and determine the single remaining parameter in the standard model [2], namely, the baryon-to-photon ratio, η. In contrast, D and ^{3}He are highly dependent on models of chemical evolution (^{3}He is in addition dependent on the uncertain stellar yields of this isotope). New data from quasar absorption systems, on what may be primordial D/H is at this time disconcordant, different measurements give different abundances. As a consequence of the uncertainties in D and ^{3}He, one can hope to use the predictions based on ^{4}He and ^{7}Li in order to construct models of galactic chemical evolution. These results also have important implications for the amount of (non)-baryonic dark matter in the galaxy and on the number of allowed relativistic degrees of freedom at the time of BBN, commonly parameterized as N_ν.

1.1. STANDARD MODEL BASICS

Since one of the main inputs of the theoretical side of BBN is the standard hot big bang model, it will be useful to review some of the key concepts as they pertain to BBN. The metric for the FLRW model of the Universe is specified by two quantities, the curvature constant k, and the expansion scale factor $R(t)$. At early times, the curvature is unimportant as can be seen from the Friedmann equation for the Hubble parameter

$$H^2 \equiv \left(\frac{\dot{R}}{R}\right)^2 = \frac{1}{3} 8\pi G_N \rho - \frac{k}{R^2} + \frac{1}{3}\Lambda \tag{1}$$

where Λ is the cosmological constant. Since the density ρ scales as either R^{-3} (for a matter dominated universe) or R^{-4} (for a radiation dominated universe), this term dominates over either the curvature or the cosmological constant. I will ignore both in what follows.

The critical energy density ρ_c is defined such that $\rho = \rho_c$ for $k = 0$

$$\rho_c = 3H^2/8\pi G_N \tag{2}$$

In terms of the present value of the Hubble parameter this is,

$$\rho_c = 1.88 \times 10^{-29} {h_o}^2 \mathrm{gcm}^{-3} \tag{3}$$

where

$$h_o = H_o/(100\text{kmMpc}^{-1}\text{s}^{-1}) \tag{4}$$

The cosmological density parameter is then defined by

$$\Omega \equiv \frac{\rho}{\rho_c} \tag{5}$$

in terms of which the Friedmann equation, Eq. (1), can be rewritten as (with $\Lambda = 0$)

$$(\Omega - 1)H^2 = \frac{k}{R^2} \tag{6}$$

so that $k = 0, +1, -1$ corresponds to $\Omega = 1, \Omega > 1$ and $\Omega < 1$. (Very) broad observational limits on h_o and Ω are

$$0.4 \leq h_o \leq 1.0 \qquad 0.1 \leq \Omega \leq 2 \tag{7}$$

The value of Ω, at least on relatively small scales, seems to depend on scale. Indeed, the contribution to Ω from visible matter associated with stars and hot gas is quite small, $\Omega \approx 0.003 - 0.01$. On somewhat larger scales, that of galactic halos or small groups of galaxies, $\Omega \approx 0.02 - 0.1$. On galaxy cluster scales, it appears that Ω may be as large as 0.3. And while there is some evidence, the observations are far from conclusive in indicating a value of Ω as large as 1. It is however possible to obtain a bound on the product, Ωh^2 from

$$H_o t_o = \int_0^1 (1 - \Omega + \Omega/x)^{-1/2} dx \tag{8}$$

(for $\Lambda = 0$). For $t_o > 12$Gyr, and $\Omega \leq 1$, $\Omega h^2 < 0.3$ (This is true even if $\Lambda \neq 0$.)

As indicated above, BBN takes place during the radiation dominated epoch which lasts roughly to the period of recombination (somewhat earlier when dark matter is included) which occurs when electrons and protons form neutral hydrogen through $e^- + p \rightarrow \text{H} + \gamma$ at a temperature $T_R \sim$ few $\times 10^3$ K $\sim$1 eV. For $T < T_R$, photons are decoupled while for $T > T_R$, photons are in thermal equilibrium. Today, the content of the microwave background consists of photons with $T_o = 2.728 \pm .002$ K [3]. The energy density of photons in the background can be calculated from

$$\rho_\gamma = \int E_\gamma dn_\gamma \tag{9}$$

where the density of states is given by

$$dn_\gamma = \frac{g_\gamma}{2\pi^2}[exp(E_\gamma/T) - 1]^{-1} q^2 dq \tag{10}$$

and $g_\gamma = 2$ is the number of spin polarizations for the photon, $E_\gamma = q$ is just the photon energy (momentum). (I am using units such that $\hbar = c = k_B = 1$ and will do so through the remainder of these lectures.) Integrating (9) gives

$$\rho_\gamma = \frac{\pi^2}{15} T^4 \tag{11}$$

which is the familiar blackbody result.

In general, at very early times, at very high temperatures, other particle degrees of freedom join the radiation background when $T \sim m_i$ for each particle type i, if that type is brought into thermal equilibrium through interactions. In equilibrium the energy density of a particle type i is given by

$$\rho_i = \int E_i dn_{q_i} \tag{12}$$

and

$$dn_{q_i} = \frac{g_i}{2\pi^2} [exp[(E_{q_i} - \mu_i)/T] \pm 1]^{-1} q^2 dq \tag{13}$$

where again g_i counts the total number of degrees of freedom for type i,

$$E_{q_i} = \left(m_i^2 + q_i^2\right)^{1/2} \tag{14}$$

μ_i is the chemical potential if present and $\pm$ corresponds to either Fermi or Bose statistics.

In the limit that $T \gg m_i$ the total energy density can be conveniently expressed by

$$\rho = \left(\sum_B g_B + \frac{7}{8} \sum_F g_F\right) \frac{\pi^2}{30} T^4 \equiv \frac{\pi^2}{30} N(T) T^4 \tag{15}$$

where $g_{B(F)}$ are the total number of boson (fermion) degrees of freedom and the sum runs over all boson (fermion) states with $m \ll T$. The factor of 7/8 is due to the difference between the Fermi and Bose integrals. Equation (15) defines N(T) by taking into account new particle degrees of freedom as the temperature is raised.

In the radiation dominated epoch, we can obtain a relationship between the age of the Universe and its temperature

$$t = \left(\frac{90}{32\pi^3 G_N N(T)}\right)^{1/2} T^{-2} \tag{16}$$

Put into a more convenient form

$$t T_{MeV}^2 = 2.4 [N(T)]^{-1/2} \tag{17}$$

TABLE 1. Effective numbers of degrees of freedom in the standard model.

Temperature	New Particles	$4N(T)$
$T < m_e$	γ's + ν's	29
$m_e < T < m_\mu$	$e^\pm$	43
$m_\mu < T < m_\pi$	$\mu^\pm$	57
$m_\pi < T < Tc^*$	π's	69
$T_c < T < m_{\rm strange}$	- π's + $u, \bar{u}, d, \bar{d}$ + gluons	205
$m_s < T < m_{charm}$	$s, \bar{s}$	247
$m_c < T < m_\tau$	$c, \bar{c}$	289
$m_\tau < T < m_{bottom}$	$\tau^\pm$	303
$m_b < T < m_{W,Z}$	$b, \bar{b}$	345
$m_{W,Z} < T < m_{top}$	$W^\pm, Z$	381
$m_t < T < m_{Higgs}$	$t, \bar{t}$	423
$M_H < T$	H^o	427

*T_c corresponds to the confinement-deconfinement transition between quarks and hadrons. $N(T)$ is shown in Figure 1 for $T_c = 150$ and 400 MeV. It has been assumed that $m_{Higgs} > m_{top}$.

where t is measured in seconds and T_{MeV} in units of MeV.

The value of $N(T)$ at any given temperature depends on the particle physics model. In the standard $SU(3) \times SU(2) \times U(1)$ model, we can specify $N(T)$ up to temperatures of 0(100) GeV. The change in N can be seen in the following table.

At higher temperatures ($T \gg 100$ GeV), $N(T)$ will be model dependent. For example, in the minimal $SU(5)$ model, one needs to add to $N(T)$, 24 states for the X and Y gauge bosons, another 24 from the adjoint Higgs, and another 6 (in addition to the 4 already counted in $W^\pm, Z$ and H) from the $\bar{5}$ of Higgs. Hence for $T > M_X$ in minimal $SU(5)$, $N(T) = 160.75$. In a supersymmetric model this would at least double, with some changes possibly necessary in the table if the lightest supersymmetric particle has a mass below M_H.

The presence of a particle species in the thermal background assumes thermal equilibrium and hence interaction rates which are sufficiently fast compared with the expansion rate of the Universe. Roughly, this translates to the condition for each particle type i, that some rate Γ_i involving that type be larger than the expansion rate of the Universe or

$$\Gamma_i > H \tag{18}$$

in order to be in thermal equilibrium.

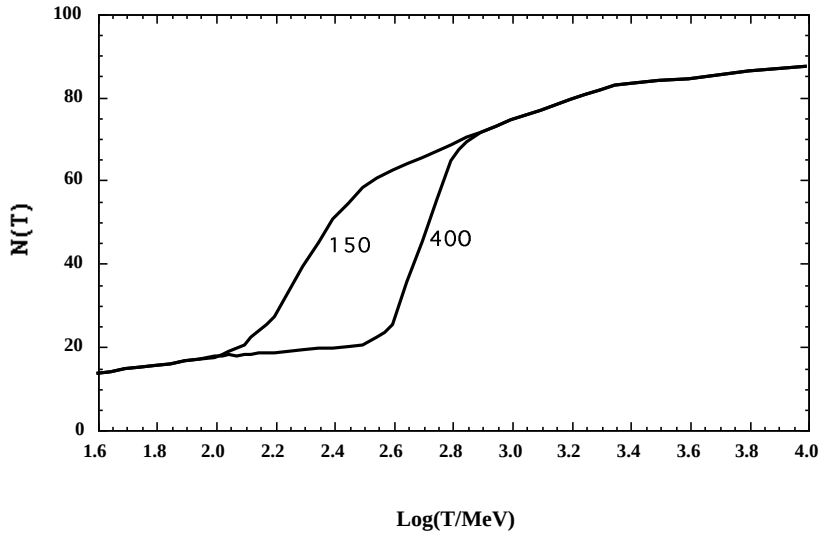

Figure 1. The effective numbers of relativistic degrees of freedom as a function of temperature.

Examples of a processes in equilibrium at early times which drops out of equilibrium or decouples at later times are the processes which involve neutrinos. If we consider the standard neutral or charged-current interactions such as $e^+ + e^- \leftrightarrow \nu + \bar{\nu}$ or $e + \nu \leftrightarrow e + \nu$ etc., the rates for these processes can be approximated by

$$\Gamma = n\langle\sigma v\rangle \tag{19}$$

where $\langle\sigma v\rangle$ is the thermally averaged weak interaction cross section

$$\langle\sigma v\rangle \sim 0(10^{-2})T^2/M_W^4 \tag{20}$$

and n is the number density of leptons. Hence the rate for these interactions is

$$\Gamma_{\rm wk} \sim 0(10^{-2})T^5/M_W^4 \tag{21}$$

The expansion rate, on the other hand, is just

$$H = \left(\frac{8\pi G_N \rho}{3}\right)^{1/2} = \left(\frac{8\pi^3}{90}N(T)\right)^{1/2} T^2/M_P \sim 1.66 N(T)^{1/2} T^2/M_P. \tag{22}$$

The Planck mass $M_P = G_N^{-1/2} = 1.22 \times 10^{19}$ GeV.

Neutrinos will be in equilibrium when $\Gamma_{\rm wk} > H$ or

$$T > (500 M_W^4)/M_P)^{1/3} \sim 1 MeV. \tag{23}$$

The temperature at which these rates are equal is commonly referred to as the decoupling or freeze-out temperature and is defined by

$$\Gamma(T_d) = H(T_d) \tag{24}$$

For temperatures $T > T_d$, neutrinos will be in equilibrium, while for $T < T_d$ they will not. Basically, in terms of their interactions, the expansion rate is just too fast and they never *"see"* the rest of the matter in the Universe (or themselves). Their momenta will simply redshift and their effective temperature (the shape of their momenta distribution is not changed from that of a blackbody) will simply fall with $T{\sim}1/R$.

Soon after decoupling the $e^{\pm}$ pairs in the thermal background begin to annihilate (when $T \lesssim m_e$). Because the neutrinos are decoupled, the energy released heats up the photon background relative to the neutrinos. The change in the photon temperature can be easily computed from entropy conservation. The neutrino entropy must be conserved separately from the entropy of interacting particles. If we denote $T_>$, the temperature of photons, and $e^{\pm}$ before annihilation, we also have $T_\nu = T_>$ as well. The entropy density of the interacting particles at $T = T_>$ is just

$$s_> = \frac{4}{3}\frac{\rho_>}{T_>} = \frac{4}{3}(2 + \frac{7}{2})(\frac{\pi^2}{30})T_>^3 \tag{25}$$

while at $T = T_<$, the temperature of the photons just after $e^{\pm}$ annihilation, the entropy density is

$$s_< = \frac{4}{3}\frac{\rho_<}{T_<} = \frac{4}{3}(2)(\frac{\pi^2}{30})T_<^3 \tag{26}$$

and by conservation of entropy $s_< = s_>$ and

$$(T_</T_>)^3 = 11/4 \tag{27}$$

Thus, the photon background is at higher temperature than the neutrinos because the $e^{\pm}$ annihilation energy could not be shared among the neutrinos, and

$$T_\nu = (4/11)^{1/3}T_\gamma \simeq 1.9K \tag{28}$$

1.2. HISTORICAL PERSPECTIVES

There has always been an intimate connection between BBN and the microwave background as a key test to the standard big bang model. Indeed, it was the formulation of BBN which predicted the existence of the microwave background radiation [4]. The argument is rather simple. BBN

requires temperatures greater than 100 keV, which according to eqs. (16) and (17) corresponds to timescales less than about 200 s. The typical cross section for the first link in the nucleosynthetic chain is

$$\sigma v(p + n \rightarrow D + \gamma) \simeq 5 \times 10^{-20} \mathrm{cm}^3/\mathrm{s} \tag{29}$$

This implies that it was necessary to achieve a density

$$n \sim \frac{1}{\sigma v t} \sim 10^{17} \mathrm{cm}^{-3} \tag{30}$$

The density in baryons today is known approximately from the density of visible matter to be $n_{Bo} \sim 10^{-7}$ cm^{-3} and since we know that that the density n scales as $R^{-3} \sim T^3$, the temperature today must be

$$T_o = (n_{Bo}/n)^{1/3} T_{\mathrm{BBN}} \sim 10\mathrm{K} \tag{31}$$

A pretty good estimate.

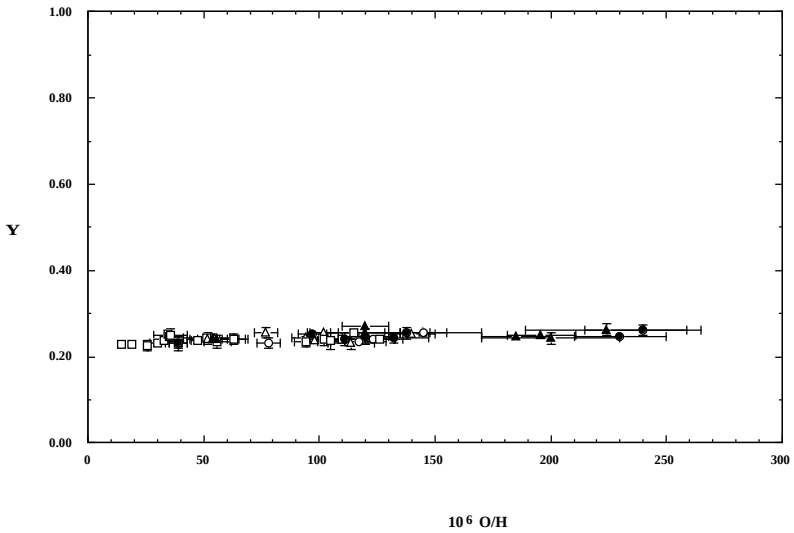

Figure 2. The helium (Y) vs oxygen (O/H) abundances in extragalactic HII regions emphasizing the lack of low ^{4}He regions.

Despite its simplicity, BBN was criticized early on, due to its shortcomings in being able to produce the observed abundances of *all* of the element isotopes due primarily to the gaps in stable nuclei at $A = 5$ and $A = 8$. Attention was therefore turned to stellar nucleosynthesis [5]. However, while the elements from helium on up can be and are produced in stars, no other astrophysical site has ever survived for the production of deuterium [6]. In

addition, if one assumes that ^{4}He is entirely of stellar origin, one should be able to find places in the Universe in which the ^{4}He mass fraction is substantially below 25%. The ^{4}He data shown in Figure 2, emphasizes the fact that indeed no such region with low ^{4}He has ever been observed and that (together with the need to produce D) leads one to conclude that BBN nucleosynthesis is a necessary component in any cosmological model. The foundations of modern BBN continued to be laid over time [7] establishing the notions of equilibrium and the nuclear network to obtain the abundances of D through ^{7}Li.

2. Theory

Conditions for the synthesis of the light elements were attained in the early Universe at temperatures $T \lesssim 1$ MeV. At somewhat higher temperatures, weak interaction rates were in equilibrium. In particular, the processes

$$\begin{aligned} n + e^+ &\leftrightarrow p + \bar{\nu}_e \\ n + \nu_e &\leftrightarrow p + e^- \\ n &\leftrightarrow p + e^- + \bar{\nu}_e \end{aligned}$$

fix the ratio of number densities of neutrons to protons. At $T \gg 1$ MeV, $(n/p) \simeq 1$. The energy density (dominated by radiation) in the standard model is

$$\rho = \frac{\pi^2}{30}(2 + \frac{7}{2} + \frac{7}{4}N_\nu)T^4 \tag{32}$$

from the contributions of photons, electrons and positrons, and N_ν neutrino flavors.

As the temperature fell and approached the point where the weak interaction rates were no longer fast enough to maintain equilibrium, the neutron to proton ratio was given approximately by the Boltzmann factor, $(n/p) \simeq e^{-\Delta m/T}$, where Δm is the neutron-proton mass difference. The final abundance of ^{4}He is very sensitive to the (n/p) ratio. As in the case of the neutrino interactions discussed above, freeze out occurs at about an MeV (slightly less than an MeV in this case).

The nucleosynthesis chain begins with the formation of deuterium through the process, $p + n \rightarrow$ D $+\gamma$. However, because the large number of photons relative to nucleons, $\eta^{-1} = n_\gamma/n_B \sim 10^{10}$, deuterium production is delayed past the point where the temperature has fallen below the deuterium binding energy, $E_B = 2.2$ MeV (the average photon energy in a blackbody is $\bar{E}_\gamma \simeq 2.7T$). The point being that there are many photons in the exponential tail of the photon energy distribution with energies $E > E_B$ despite the fact that the temperature or $\bar{E}_\gamma$ are less than E_B. This can be seen

by comparing the qualitative expressions for the deuterium production and destruction rates,

$$\begin{aligned} \Gamma_p &\approx n_B \sigma v \\ \Gamma_d &\approx n_\gamma \sigma v e^{-E_B/T} \end{aligned} \tag{33}$$

When the quantity $\eta^{-1}\exp(-E_B/T) \sim 1$ the rate for deuterium destruction (D $+\gamma \rightarrow p + n$) finally falls below the deuterium production rate and the nuclear chain begins at a temperature $T \sim 0.1 MeV$.

In addition to the $p\ (n, \gamma)$ D reaction, the other major reactions leading to the production of the light elements are:

D (D, p) T D (n, γ) T ^{3}He $(n,\ p)$ T
D (D, n) ^{3}He D (p, γ) ^{3}He

Followed by the reactions producing ^{4}He:

D (D, γ) ^{4}He ^{3}He (^{3}He, $2p$) ^{4}He
D (^{3}He, p) ^{4}He T (p, γ) ^{4}He
T (D, n) ^{4}He ^{3}He (n, γ) ^{4}He

The gap at $A = 5$ is overcome and the production of ^{7}Li proceeds through:

^{3}He (^{4}He,γ) ^{7}Be
$\rightarrow {}^7\mathrm{Li} + e^+ + \nu_e$
T (^{4}He,γ) ^{7}Li

The gap at $A = 8$ prevents the production of other isotopes in any significant quantity. The nuclear chain in BBN calculations was extended [8] and is shown in Figure 3.

The dominant product of big bang nucleosynthesis is ^{4}He resulting in an abundance of close to 25% by mass. This quantity is easily estimated by counting the number of neutrons present when nucleosynthesis begins. When the weak interaction rates responsible for $n - p$ equilibrium freeze-out, at $T \approx 0.8$ MeV, the neutron to proton ratio is about 1/6. When free neutron decays prior to deuterium formation are taken into account, the ratio drops to $(n/p) \approx 1/7$. Then simple counting yields a ^{4}He mass fraction

$$Y_p = \frac{2(n/p)}{[1 + (n/p)]} \approx 0.25 \tag{34}$$

In the standard model with $N_\nu = 3$, there is basically one free parameter in BBN, namely the baryon to photon ratio, η. As we have seen above, the value of η controls the onset of nucleosynthesis through the deuterium bottleneck. For larger values of η, the quantity $\eta^{-1}\exp(-E_B/T)$ is smaller, and hence the nuclear chain may begin at a higher temperature. Remember also that a key ingredient in determining the final mass fraction of ^{4}He, is (n/p) [see eq. (34)] and that the final value of (n/p) was determined by the

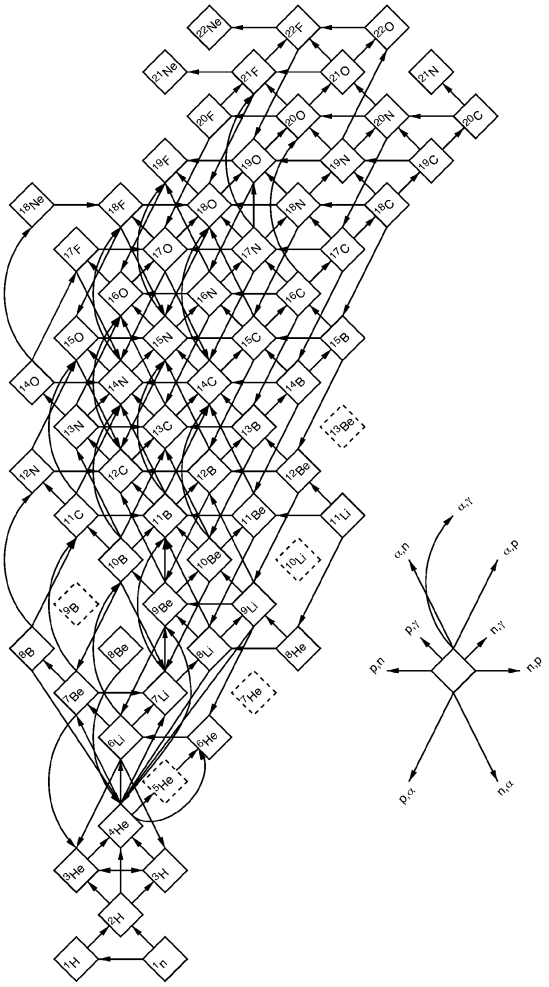

Figure 3. The nuclear network used in BBN calculations.

time at which nucleosynthesis begins, thus controlling the time available for free decays after freeze out. If nucleosynthesis begins earlier, this leaves less time for neutrons to decay and the value of (n/p) and hence Y_p is increased. But because the (n/p) ratio is only weakly dependent on η, the ^{4}He mass fraction is relatively flat as a function of η. When we go beyond the standard

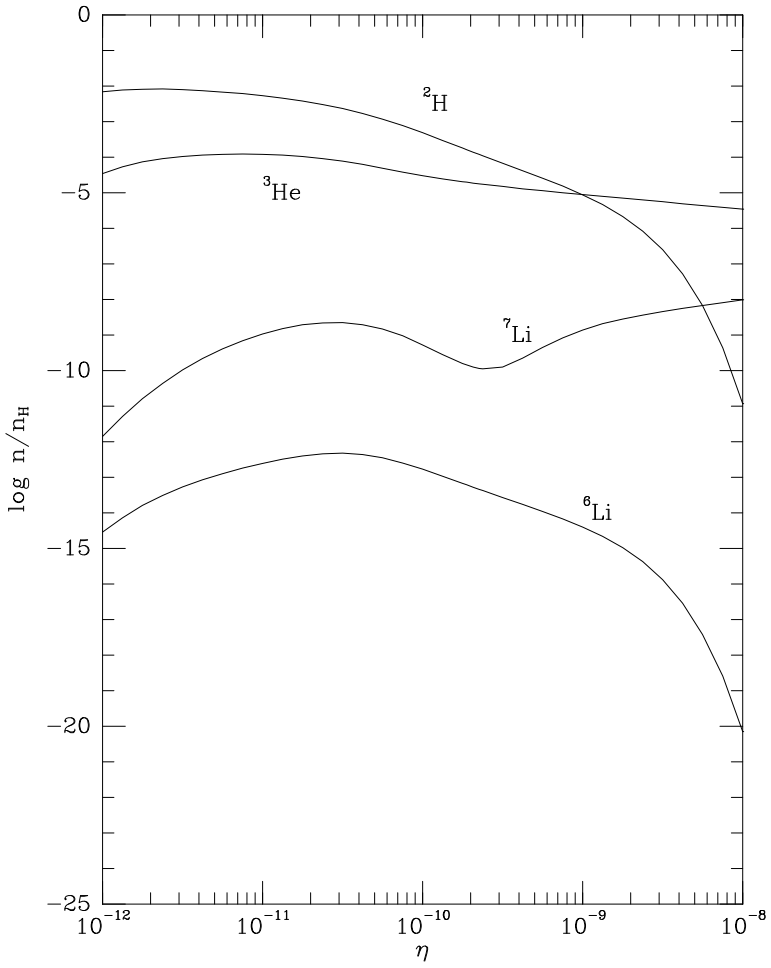

Figure 4. The light element abundances from big bang nucleosynthesis as a function of η, including ^{6}Li.

model, the ^{4}He abundance is very sensitive to changes in the expansion rate which can be related to the effective number of neutrino flavors as will be discussed below. Lesser amounts of the other light elements are produced: D and ^{3}He at the level of about 10^{-5} by number, and ^{7}Li at the level of 10^{-10} by number. These abundances (along with ^{6}Li) are shown in Figure 4 [8]. In Figure 5, the produced abundances of the intermediate mass

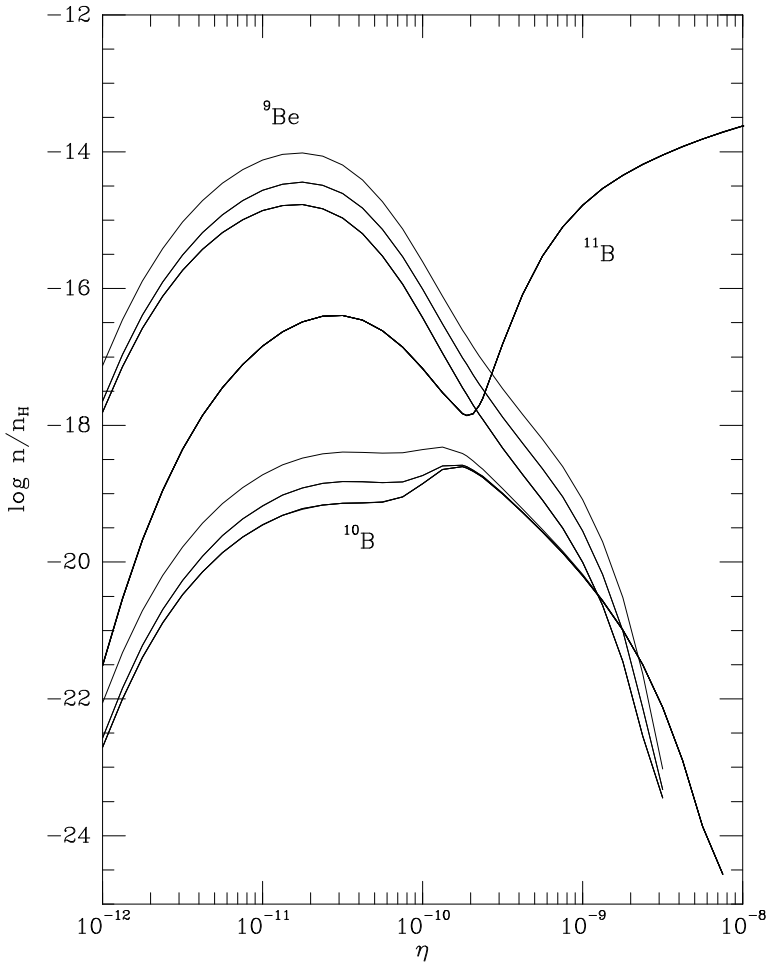

Figure 5. The intermediate mass element abundances from big bang nucleosynthesis as a function of η.

isotopes ^{9}Be, ^{10}B, ^{11}B are also shown. These abundances are far below the observed values and it is believed that these isotopes are formed in cosmic ray nucleosynthesis.

It is perhaps convenient at this time to note that the value of η is directly

related to the fraction of Ω in baryons. Indeed, one can write

$$\Omega_B h^2 = 3.67 \times 10^7 \eta (T_0/2.728\mathrm{K})^3 \tag{35}$$

where T_0 is the present temperature of the microwave background.

Historically, it has been common to refer to two other parameter in BBN, the neutron mean life and the number of neutrino flavors. The neutron mean life is now very well determined and its remaining uncertainty can be treated simply as an uncertainty in the calculated abundance of ^{4}He. Although the number of neutrino flavors has also been fixed experimentally, BBN is sensitive to the number of light degrees of freedom whether or not they interact weakly. It is often convenient to refer to these degrees of freedom as neutrino equivalents. By increasing N_ν in eq. (32), one increases the expansion rate $H \propto \sqrt{\rho}$. As a result, the weak interactions freeze-out at a higher temperature (see eqs. (21) and (22)). This leads once again to a higher value for (n/p) and a higher ^{4}He mass fraction. This effect will be treated in more detail in the last lecture.

For the comparison with the observations, I will use the resulting abundances of the light elements shown in Figure 6, which concentrate on the range in η_{10} between 1 and 10. The curves for the ^{4}He mass fraction, Y, bracket the computed range based on the uncertainty of the neutron mean-life which has been taken as [9] $\tau_n = 887 \pm 2$ s. Uncertainties in the produced ^{7}Li abundances have been adopted from the results in Hata et al. [10]. Uncertainties in D and ^{3}He production are small on the scale of this figure. The boxes correspond to the observed abundances and will be discussed below.

3. Abundances

3.1. ^{4}He

^{4}He is produced in stars, therefore to be able to extract a primordial abundance of ^{4}He, it is advantageous to make abundance measurements in systems of very low metallicity. Low metallicity or low abundances of C, N, and O relative to the solar abundances of these elements would indicate that the level of stellar processing is minimized. The ^{4}He abundance in very low metallicity regions is best determined from observations of HeII $\rightarrow$ HeI recombination lines in extragalactic HII (ionized hydrogen) regions. There is now a good collection of abundance information on the ^{4}He mass fraction, Y, O/H, and N/H in over 70 [11, 12, 13] such regions. In an extensive study based on the data in [11, 12], it was found [14] that the data is well represented by a linear correlation for Y vs. O/H and Y vs. N/H. It is then expected that the primordial abundance of ^{4}He can be determined from the intercept of that relation. A detailed analysis of the data including

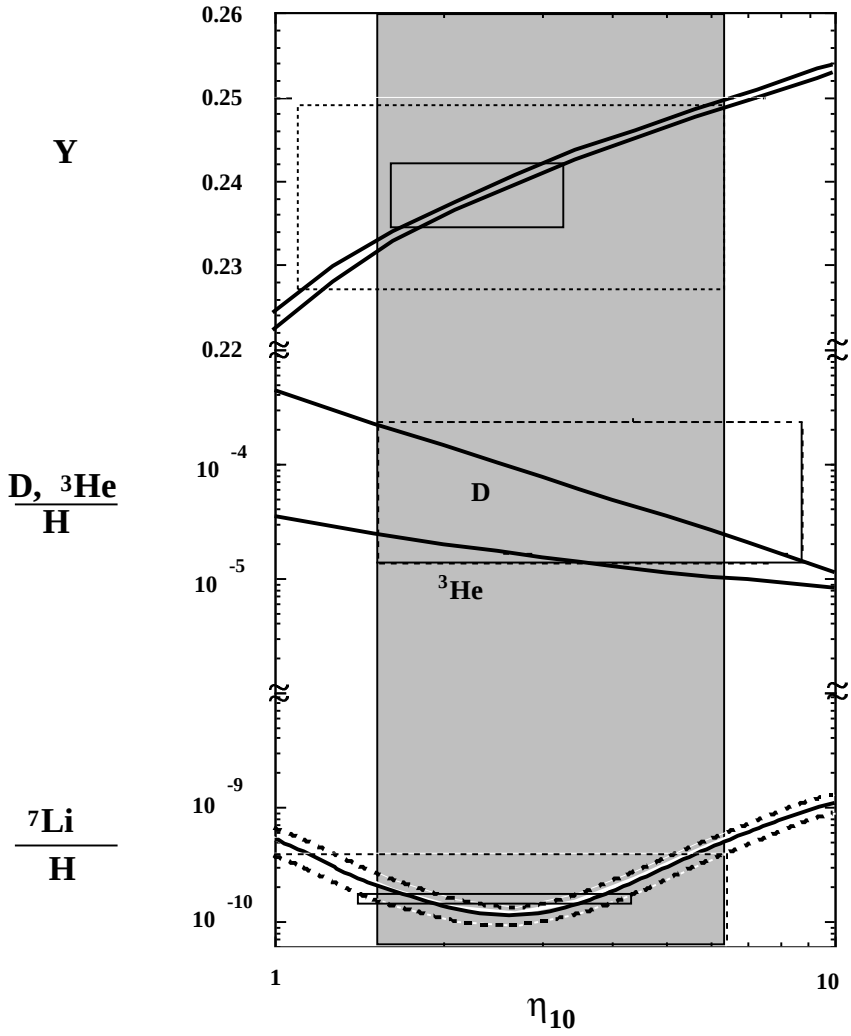

Figure 6. The light element abundances from big bang nucleosynthesis as a function of $\eta_{10} = 10^{10}\eta$.

that in [13] found an intercept corresponding to a primordial abundance $Y_p = 0.234 \pm 0.002 \pm 0.005$ [15]. The stability of this fit was verified by a statistical bootstrap analysis [16] showing that the fits were not overly sensitive to any particular HII region.

To make use of the ^{4}He data, it is crucial to obtain high quality and very low metallicity data. In principle, any one HII region (with non-zero metallicity) should provide an upper limit to Y_p since some stellar processing has

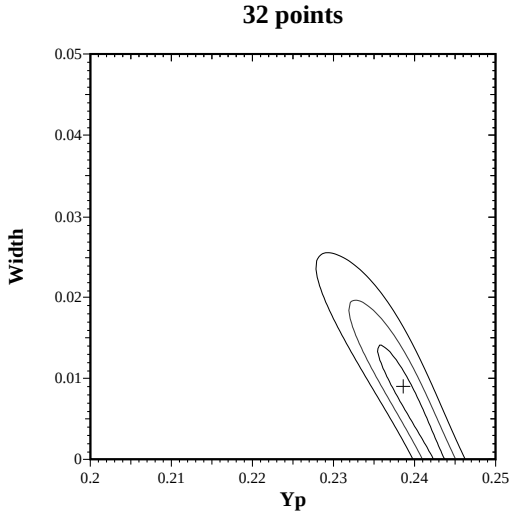

Figure 7. Equal likelihood 1, 2, and 3 σ contours in the $w - Y_p$ plane. The cross shows the position of the peak of the likelihood function.

taken place augmenting the primordial value. Thus the determination of Y_p by an extrapolation to zero metallicity could be avoided by the observations of either low metallicity or low helium HII regions. For a very low metallicity HII region such an upper limit may even provide a reasonable estimate of Y_p.

Another way to avoid an extrapolation to zero metallicity (though such an extrapolation is in fact quite minimal given the low metallicity data available), one can perform a Bayesian analysis [17] in which one makes no other assumption other than the observed ^{4}He abundance is greater than or equal to the primordial abundance. That is, one can consider three quantities: Y_T, the true ^{4}He abundance in an H II region about which the observed abundance Y_O is distributed. Both of these differ from the primordial abundance Y_p and the only prior assumed is that for each object, $Y_T \geq Y_p$. If we assume that the true abundance differs from the primordial abundance by no more than w, we can derive a total likelihood function by integrating out the unknown Y_T. We can then plot the equal likelihood contours as a function of Y_p and w. This is shown in Figure 7, where the 32 points of lowest metallicity have been used to calculate the likelihood

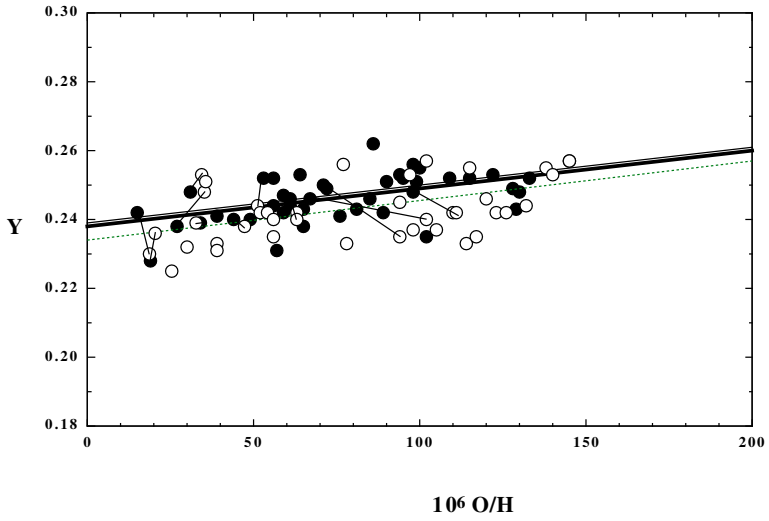

Figure 8. The helium (Y) and oxygen (O/H) abundances in extragalactic HII regions, from refs. [11, 12] (open circles), and from ref. [18] (filled circles). Lines connect the same regions observed by different groups.

function. The peak occurs at $Y_p = 0.238$ and the most likely width is $w = 0.009$. The 95% CL upper limit to Y_p in this case is 0.245. For further details on this approach see [17]. The data used in Figure 7 represents an update of that work and includes the data of ref. [18].

Although the above estimates on Y_p are consistent with those based on a linear extrapolation of the data, it has been claimed that the new data in refs. [13] and [18] leads to a significantly higher value for Y_p (in excess of 24%). The higher values of Y_p, quoted by Izotov and Thuan are based on their ^{4}He abundances derived by their method of determining all of the parameters from a set of 5 helium recombination lines. This gives $Y_p = 0.2444 \pm 0.0015 + (44 \pm 19)$O/H. However, as argued in [15] there are inherent uncertainties in this method which are not reflected in the error budget. For this reason and because we can more easily compare their data with previous data, we use their results which are based on S II densities. These results are entirely consistent with the data in refs. [11, 12] as can be seen in Figure 8 where the Y versus O/H data from refs. [11, 12] (open circles) is shown along with the newer data (filled circles, from ref. [18]). The fit to the open circles is shown by the dashed line with intercept 0.234, the fit to the filled circles is shown by the this solid line (barely visible) with intercept 0.239. Combining all the data one finds [19] a ^{4}He mass fraction based on 73 distinct HII regions

$$Y_p = 0.238 \pm 0.002 \pm 0.005 \tag{36}$$

The first uncertainty is purely statistical and the second uncertainty is an estimate of the systematic uncertainty in the primordial abundance determination [15]. The fit to all the data is shown by the thick line with intercept given by Eq. (36) above. The small errors quoted in [18] account for the total fit being skewed to the higher value of Y_p. The solid box for ^{4}He in Figure 6 represents the range (at $2\sigma_{\rm stat}$) from (36). The dashed box extends this by including the systematic uncertainty. A somewhat lower primordial abundance of $Y_p = 0.235 \pm .003$ is found by restricting to the 36 most metal poor regions [19].

The primordial ^{4}He abundance can also be determined by examining the correlation between Y and N/H. Indeed in all but one of the H II regions, N/H data is also available. However, unless N/H is directly proportional to O/H, it is not clear that a linear Y vs. N/H fit should give the same result. Indeed, the proportionality of N/H to O/H (or in other terms the primary vs secondary nature of nitrogen) has been studied [14, 15, 19]. Unfortunately from a theoretical point of view this question lies in the realm of very uncertain yields for nitrogen in AGB stars. The data indicate that N is mostly primary. Though the secondary contribution may be responsible for yielding systematically higher intercepts for Y vs N/H relative to Y vs. O/H, however the difference is small $\lesssim 0.003$.

Finally, it also of interest to test our understanding of the slope in the Y vs. O/H data. The data overall show a relatively steep slope $\Delta Y/\Delta O \simeq 110 \pm 25$. Models of chemical evolution typically give a much smaller value of about 20 and even in models with outflow (material ejected from the galaxy) the slopes only go up to about 60. This question, like the N vs. O question is highly sensitive to very uncertain theoretical yields [19].

3.2. ^{7}Li

The ^{7}Li abundance is also reasonably well known. In old, hot, population-II stars, ^{7}Li is found to have a very nearly uniform abundance [20]. For stars with a surface temperature $T > 5500$ K and a metallicity less than about 1/20th solar (so that effects such as stellar convection may not be important), the abundances show little or no dispersion beyond that which is consistent with the errors of individual measurements. Indeed, as detailed in ref. [21], much of the work concerning ^{7}Li has to do with the presence or absence of dispersion and whether or not there is in fact some tiny slope to a [Li] = log ^{7}Li/H + 12 vs. T or [Li] vs. [Fe/H] relationship ([Fe/H] is the log of the Fe/H ratio relative to the solar value).

There is ^{7}Li data from nearly 100 halo stars, from a variety of sources. When the Li data from stars with [Fe/H] < -1.3 is plotted as a function of surface temperature, one sees a plateau emerging for $T > 5500$ K as shown

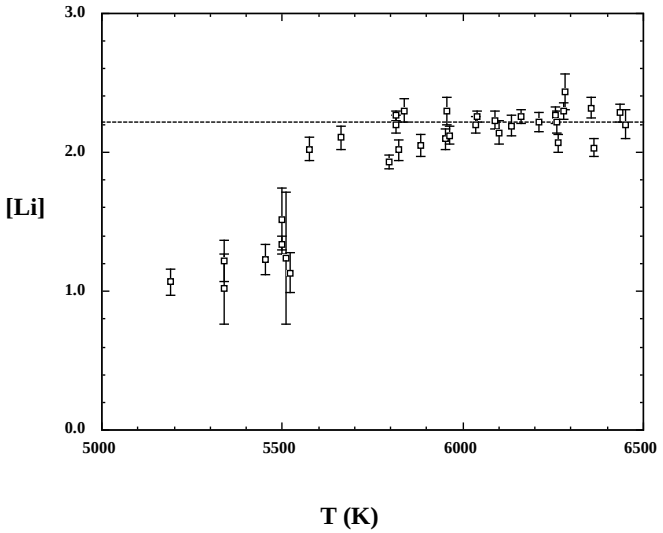

Figure 9. The Li abundance in halo stars with [Fe/H] < -1.3, as a function of surface temperature. The dashed line shows the value of the weighted mean of the plateau data.

in Figure 9 for the data taken from ref. [21]. As one can see from the figure, at high temperatures, where the convection zone does not go deep below the surface, the Li abundance is uniform. At lower temperatures, the surface abundance of Li is depleted as Li passes through the hotter interior of the star and is destroyed. The lack of dispersion in the plateau region is evidence that this abundance is indeed primordial (or at least very close to it). Another way to see the plateau is to plot the Li abundance data as a function of metallicity, this time with the restriction that $T > 5500$ K as seen in Figure 10. In this case, the plateau emerges at low [Fe/H] as would be expected. At higher [Fe/H], the convection zone remains near the surface only for much hotter stars. Thus, for [Fe/H] > -1.3, the effects of depletion are seen. Also apparent in this figure is that at higher metallicities there is evidence for the production of Li which rises by over an order of magnitude at solar metallicity.

I will use the value given in ref. [21] as the best estimate for the mean ^{7}Li abundance and its statistical uncertainty in halo stars

$$\mathrm{Li/H} = (1.6 \pm 0.1) \times 10^{-10} \tag{37}$$

The Li abundance determination is sensitive to stellar parameters such as the assumed surface temperature, the metallicity and the surface gravity. The greatest model dependence is on the conversion of the observed colors (B-V) to temperature. For example, in a sample of 55 stars taken from the papers of ref. [20], one finds [Li] $= 2.08 \pm 0.02$. From Thorburn's[22]

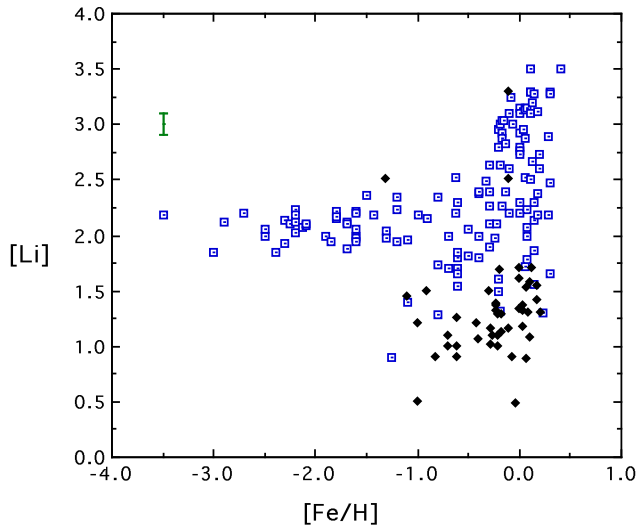

Figure 10. The Li abundance in halo stars with $T > 5500$ K, as a function of metallicity. Filled diamonds represent upper limits.

sample of 74 stars one finds [Li] $= 2.26 \pm 0.01$. I believe that much of this systematic uncertainty has now been relieved by newer methods for determining the stellar parameters and the Li abundance. The two papers in ref. [21], are based on different methods. The first uses temperatures which are determined by observations of Balmer lines [23] and the second employs the infra-red flux method [24]. The data sets in these papers which contain 24 and 41 stars respectively, both give [Li] $= 2.21 \pm 0.01$. The Li abundance used in (37) corresponds to this value. In fact when correlated with respect to either temperature or iron, the data in the latter paper of [21] shows no statistical trend. With respect to temperature, the data give [Li] $= 1.28 \pm 0.43 + (0.015 + 0.007)T/100\text{K}$, indicating a change in [Li] well within the data over the observed temperature range. With respect to iron, no slope is found [Li] $= 2.17 \pm 0.07 + (-0.018 \pm 0.031)$[Fe/H]. The variance in the plateau data is less than 0.01. The solid box for ^{7}Li in Figure 6 represents the $2\sigma_{\text{stat}}$ range from (37).

There is however an important source of systematic error due to the possibility that Li has been depleted in these stars from their initial abundance. These uncertainties are however limited. As was noted above, the lack of dispersion in the Li data limits the amount of depletion. In addition, standard stellar models[25] predict that any depletion of ^{7}Li would be accompanied by a very severe depletion of ^{6}Li. Until recently, ^{6}Li had never been observed in hot pop II stars. The observation[26] of ^{6}Li (which turns out to be consistent with its origin in cosmic-ray nucleosynthesis and

with a small amount of depletion as expected from standard stellar models) is another good indication that ^{7}Li has not been destroyed in these stars[27, 28, 29].

Aside from the big bang, Li is produced together with Be and B in cosmic ray spallation of C,N,O by protons and α-particles. Li is also produced by $\alpha - \alpha$ fusion. Be and B have been observed in these same pop II stars and in particular there are a dozen or so stars in which both Be and ^{7}Li have been observed. Thus Be (and B though there is still a paucity of data) can be used as a consistency check on primordial Li [30]. Based on the Be abundance found in these stars, one can conclude that no more than 10-20% of the ^{7}Li is due to cosmic ray nucleosynthesis leaving the remainder (an abundance near 10^{-10}) as primordial. The dashed box in Figure 6, accounts for the possibility that as much as half of the primordial ^{7}Li has been destroyed in stars, and that as much as 20% of the observed ^{7}Li may have been produced in cosmic ray collisions rather than in the Big Bang. For ^{7}Li, the uncertainties are clearly dominated by systematic effects.

3.3. D

Turning to D/H, we have three basic types of abundance information: 1) ISM data, 2) solar system information, and perhaps 3) a primordial abundance from quasar absorption systems. The best measurement for ISM D/H is [31]

$$(\mathrm{D/H})_{\mathrm{ISM}} = 1.60 \pm 0.09^{+0.05}_{-0.10} \times 10^{-5} \tag{38}$$

Because there are no known astrophysical sites for the production of deuterium, all observed D must be primordial. As a result, a firm lower bound from deuterium establishes an upper bound on η which is robust and is shown by the lower right of the solid box in Figure 6. The solar abundance of D/H is inferred from two distinct measurements of ^{3}He. The solar wind measurements of ^{3}He as well as the low temperature components of stepwise heating measurements of ^{3}He in meteorites yield the presolar (D + ^{3}He)/H ratio, as D was efficiently burned to ^{3}He in the Sun's pre-main-sequence phase. These measurements indicate that [32, 33]

$$\left(\frac{\mathrm{D} + {}^3\mathrm{He}}{\mathrm{H}}\right)_\odot = (4.1 \pm 0.6 \pm 1.4) \times 10^{-5} \tag{39}$$

The high temperature components in meteorites are believed to yield the true solar ^{3}He/H ratio of [32, 33]

$$\left(\frac{{}^3\mathrm{He}}{\mathrm{H}}\right)_\odot = (1.5 \pm 0.2 \pm 0.3) \times 10^{-5} \tag{40}$$

The difference between these two abundances reveals the presolar D/H ratio, giving,

$$(\mathrm{D/H})_\odot \approx (2.6 \pm 0.6 \pm 1.4) \times 10^{-5} \tag{41}$$

It should be noted that measurements of surface abundances of HD on Jupiter show a somewhat higher value for D/H, D/H $= 5 \pm 2 \times 10^{-5}$ [34]. If this value is confirmed and if fractionation does not significantly alter the D/H ratio (as it was suspected to for previous measurements involving CH_3D), it may have an important impact on galactic chemical evolution models. This value is marginally consistent with the inferred meteoritic values.

Finally, there have been several reported measurements of D/H in high redshift quasar absorption systems. Such measurements are in principle capable of determining the primordial value for D/H and hence η, because of the strong and monotonic dependence of D/H on η. However, at present, detections of D/H using quasar absorption systems do not yield a conclusive value for D/H. As such, it should be cautioned that these values may not turn out to represent the true primordial value and it is very unlikely that both are primordial and indicate an inhomogeneity [35] (a large scale inhomogeneity of the magnitude required to placate all observations is excluded by the isotropy of the microwave background radiation). The first of these measurements [36] indicated a rather high D/H ratio, D/H ≈ 1.9 – 2.5×10^{-4}. Other high D/H ratios were reported in [37]. More recently, a similarly high value of D/H $= 2.0 \pm 0.5 \times 10^{-4}$ was reported in a relatively low redshift system (making it less suspect to interloper problems) [38]. However, there are reported low values of D/H in other such systems [39] with values of D/H originally reported as low as $\simeq 2.5 \times 10^{-5}$, significantly lower than the ones quoted above. The abundance in these systems has been revised upwards to about $3.4 \pm 0.3 \times 10^{-5}$ [40]. I will not enter into the debate as to which if any of these observations may be a better representation of the true primordial D/H ratio. I only note that it remains a highly contested issue [40, 41] The range of quasar absorber D/H is shown by the dashed box in Figure 6.

There are also several types of ^{3}He measurements. As noted above, meteoritic extractions yield a presolar value for ^{3}He/H as given in Eq. (40). In addition, there are several ISM measurements of ^{3}He in galactic HII regions [42] which show a wide dispersion which may be indicative of pollution or a bias [43]

$$\left(\frac{^3\mathrm{He}}{\mathrm{H}}\right)_{\mathrm{HII}} \simeq 1 - 5 \times 10^{-5} \tag{42}$$

There is also a recent ISM measurement of ^{3}He [44] with

$$\left(\frac{^3\mathrm{He}}{\mathrm{H}}\right)_{\mathrm{ISM}} = 2.1^{+.9}_{-.8} \times 10^{-5} \tag{43}$$

Finally there are observations of ^{3}He in planetary nebulae [45] which show a very high ^{3}He abundance of $^3\mathrm{He/H} \sim 10^{-3}$.

Each of the light element isotopes can be made consistent with theory for a specific range in η. Overall consistency of course requires that the range in η agree among all four light elements. However, as will be argued below D and ^{3}He are far more sensitive to chemical evolution than ^{4}He or ^{7}Li and as such the direct comparison between the theoretical predictions of the primordial abundances of D and ^{3}He with the observational determination of their abundances is far more difficult. Therefore in what follows I will for the most part restrict the comparison between theory and observation to the two isotopes who suffer the least from the effects of chemical evolution.

4. Chemical Evolution

Because we can not directly measure the primordial abundances of any of the light element isotopes, we are required to make some assumptions concerning the evolution of these isotopes. As has been discussed above, ^{4}He is produced in stars along with oxygen and nitrogen. ^{7}Li can be destroyed in stars and produced in several (though still uncertain) environments. D is totally destroyed in the star formation process and ^{3}He is both produced and destroyed in stars with fairly uncertain yields. It is therefore preferable, if possible to observe the light element isotopes in a low metallicity environment. Such is the case with ^{4}He and ^{7}Li, and we can be fairly assured that the abundance determinations of these isotopes are close to primordial. If the quasar absorption system measurements of D/H stabilize, then this too may be very close to a primordial measurement. Otherwise, to match the solar and present abundances of D and ^{3}He to their primordial values requires a model of galactic chemical evolution.

The main inputs to chemical evolution models are: 1) The initial mass function, $\phi(m)$, indicating the distribution of stellar masses. Typically, a simple power law form for the IMF is chosen, $\phi(m) \sim m^{-x}$, with $x \simeq -2.7$. This is a fairly good representation of the observed distribution, particularly at larger masses. 2) The star formation rate, ψ. Typical choices for a SFR are $\psi(t) \propto \sigma$ or σ^2 or even a straight exponential $e^{-t/\tau}$. σ is the fraction of mass in gas, $M_{\mathrm{gas}}/M_{\mathrm{tot}}$. 3) The presence of infalling or outflowing gas; and of course 4) the stellar yields. It is the latter, particularly in the case of ^{3}He, that is the cause for so much uncertainty. Chemical evolution models simply set up a series of evolution equations which trace desired quantities.

For example, the mass in gas and the SFR evolve through a relation such as

$$\frac{dM_{\rm gas}}{dt} = -\psi(t) + e(t) + i(t) - o(t) \tag{44}$$

where e represents the amount of gas ejected from stars, i is the gas infall rate, and o is the gas outflow rate. The ejection rate is in turn given by

$$e(t) = \int (m - m_R)\phi(m)\psi(t - \tau(m))dm \tag{45}$$

where m_R is the remnant mass (a function of the stellar mass m as well) and $\tau(m)$ is the stellar lifetime. If we ignore $\tau(m)$, then the ejection rate is simply proportional to the star formation rate ψ, $e(t) = R\psi$. R is referred to as the return fraction and this approximation is known as the instantaneous recycling approximation (IRA). Similar equations can be developed which trace the abundances of the element isotopes [46]. Neglecting both infall and outflow, these take the form

$$\frac{d(XM_{\rm gas})}{dt} = -\psi(t)X + e_X(t) \tag{46}$$

where X is the mass fraction of a particular element of interest and e_X is the mass fraction of the element ejected in the death of a star. In the case of deuterium, $e_D = 0$.

As one can see from (46) deuterium is always a monotonically decreasing function of time in chemical evolution models. The degree to which D is destroyed, is however a model dependent question which depends sensitively on the IMF and SFR. The evolution of ^{3}He is however considerably more complicated. Stellar models predict that substantial amounts of ^{3}He are produced in stars between 1 and 3 $M_\odot$. For $M < 8M_\odot$, Iben and Truran [47] calculate

$$(^3{\rm He/H})_f = 1.8 \times 10^{-4} \left(\frac{M_\odot}{M}\right)^2 + 0.7 \left[({\rm D} + {}^3{\rm He})/{\rm H}\right]_i \tag{47}$$

so that for example, when $\eta_{10} = 3$, $({\rm (D} + {}^3{\rm He)/H})_i = 9 \times 10^{-5}$, and the ratio of the final abundance of ^{3}He/H to the initial (D + ^{3}He)/H abundance denoted by g_3 is $g_3(1M_\odot) = 2.7$. The ^{3}He abundance is nearly tripled. It should be emphasized that this prediction is in fact consistent with the observation of high ^{3}He/H in planetary nebulae [45].

Generally, implementation of the ^{3}He yield in Eq. (47) in chemical evolution models leads to an overproduction of ^{3}He/H particularly at the solar epoch [43, 48]. For example, in Figure 11, the evolution of D and ^{3}He is shown for a model in which only a modest amount of deuterium is destroyed. Namely, by a factor of 5, from D/H = 7.5 $\times 10^{-5}$ to a present

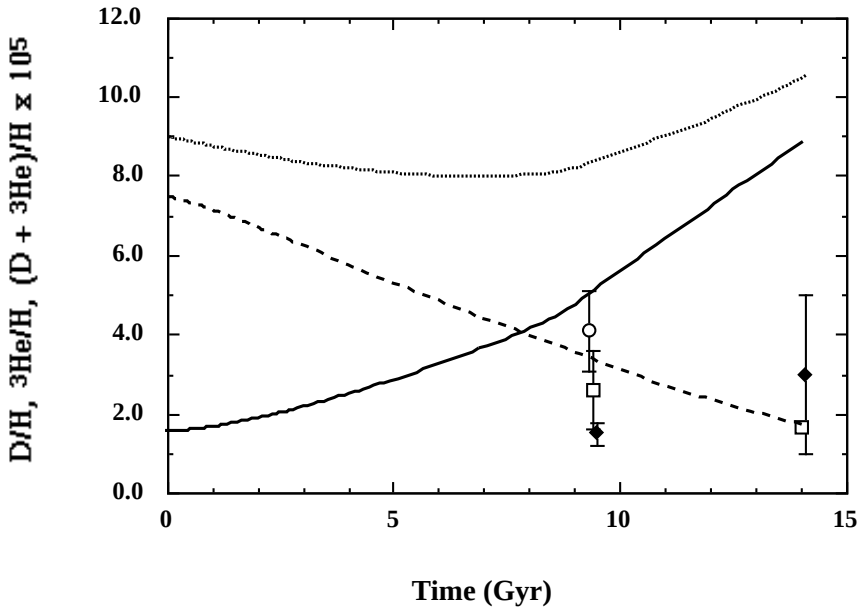

Figure 11. The evolution of D/H and ^{3}He/H and (D+^{3}He)/H with time in units of 10^{-5}. The assumed primordial abundance of D/H is 7.5 $\times 10^{-5}$. The solid curve shows the evolution of ^{3}He/H, the dashed curve for D/H and the dotted curve for the sum (D+^{3}He)/H. The diamonds show the data for ^{3}He, the open squares for deuterium and the open circle for the sum.

value of $\sim 1.5 \times 10^{-5}$. However, due to the production of ^{3}He in low mass stars, ^{3}He is greatly overproduced relative to the solar value. This problem is compounded in models with an intense period of D destruction. In Scully et al. [49], a dynamically generated supernovae wind model was coupled to models of galactic chemical evolution with the aim of reducing a primordial D/H abundance of 2 $\times 10^{-4}$ to the present ISM value without overproducing heavy elements and remaining consistent with the other observational constraints typically imposed on such models. In Figure 12, the evolution of D/H and ^{3}He/H is shown as a function of time in several representative models with significant deuterium destruction factors (see ref [49] for details). However, as one can plainly see, ^{3}He is grossly overproduced (the deuterium data is represented by squares and ^{3}He by circles).

The overproduction of ^{3}He relative to the solar meteoritic value seems to be a generic feature of chemical evolution models when ^{3}He production in low mass stars is included. This result appears to be independent of the chemical evolution model and is directly related to the assumed stellar yields of ^{3}He. It has recently been suggested that at least some low mass

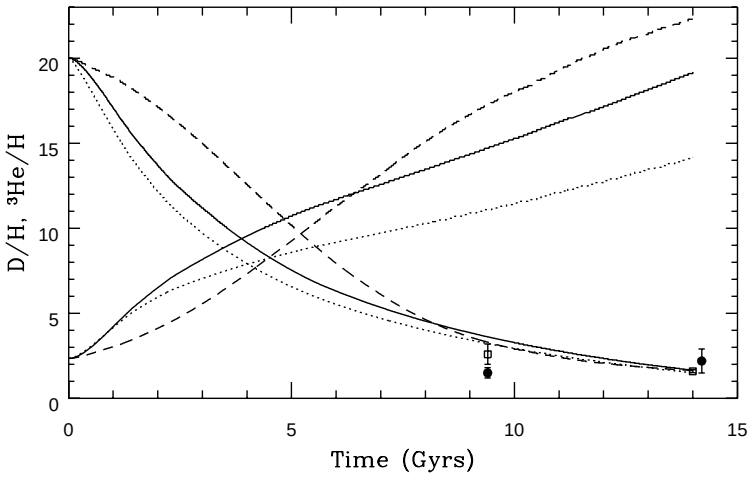

Figure 12. As in Figure 11. The primordial abundance of D/H in this case was chosen to be 2×10^{-4}.

stars may indeed be net destroyers of ^{3}He if one includes the effects of extra mixing below the conventional convection zone in low mass stars on the red giant branch [50, 51]. The extra mixing does not take place for stars which do not undergo a helium core flash (i.e. stars $>$ 1.7 - 2 $M_\odot$). Thus stars with masses *less than* 1.7 $M_\odot$ are responsible for the ^{3}He destruction. Using the yields of Boothroyd and Malaney [51], it was shown [52] that these reduced ^{3}He yields in low mass stars can account for the relatively low solar and present day ^{3}He/H abundances observed. In fact, in some cases, ^{3}He was underproduced. To account for the ^{3}He evolution and the fact that some low mass stars must be producers of ^{3}He as indicated by the planetary nebulae data, it was suggested that the new yields apply only to a fraction (albeit large) of low mass stars [52, 53]. The corresponding evolution [52] of D/H and ^{3}He/H is shown in Figure 13.

The models of chemical evolution discussed above indicate that it is possible to destroy significant amounts of deuterium and remain consistent with chemical evolutionary constraints. To do so however, comes with a price. Large deuterium destruction factors require substantial amounts of stellar processing, which at the same time produce heavy elements. To keep the heavy element abundances in the Galaxy in check, significant Galactic winds enriched in heavy elements must be incorporated. In fact there is some evidence that enriched winds were operative in the early Galaxy. In the X-ray cluster satellites observed by Mushotzky et al. [54] and Loewenstein and Mushotzky [55] the mean oxygen abundance was found to

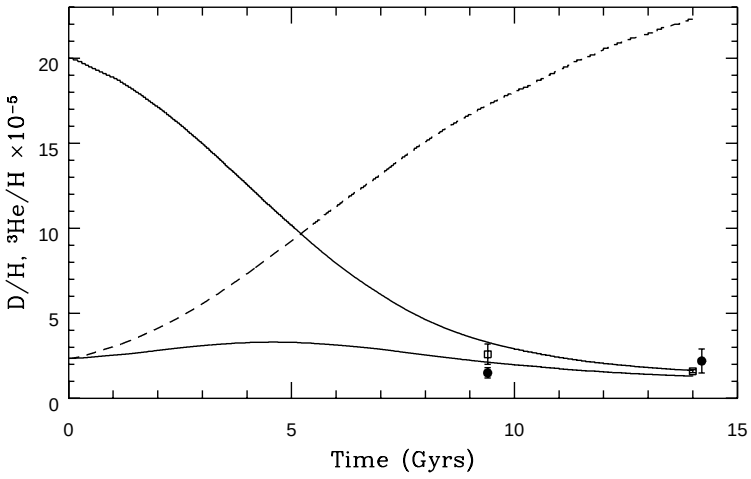

Figure 13. The evolution of D/H and ^{3}He/H with time using the reduced ^{3}He yields of ref. [51] The dashed curve is the same as in Figure 12, using standard ^{3}He yields.

be roughly half solar. This corresponds to a near solar abundance of heavy elements in the inter-Galactic medium, where apparently little or no star formation has taken place.

If our Galaxy is typical in the Universe, then the models of the type discussed above would indicate that the luminosity density of the Universe at high redshift should also be substantial augmented relative to the present. Recent observations of the luminosity density at high redshift [56] are making it possible for the first time to test models of cosmic chemical evolution. The high redshift observations, are very discriminatory with respect to a given SFR [57]. Models in which the star formation rate is proportional to the gas mass fraction (these are common place in Galactic chemical evolution) have difficulties to fit the multi-color data from $z = 0$ to 1. This includes many of the successful Galactic infall models. In contrast, models with a steeply decreasing SFR are favored. In Figure 14, the predicted luminosity density based on the model with evolution shown in Figure 13 from [49], as compared with the observations (see ref. [57] for details).

While it would be premature to conclude that all models with large deuterium destruction factors are favored, it does seem that models which do fit the high redshift data destroy significant amounts of D/H. On the other hand, we can not exclude models which destroy only a small amount of D/H as Galactic models of chemical evolution. In this case, however the evolution of our Galaxy is anomalous with respect to the cosmic average. If the low D/H measurements [39, 40] hold up, then it would seem

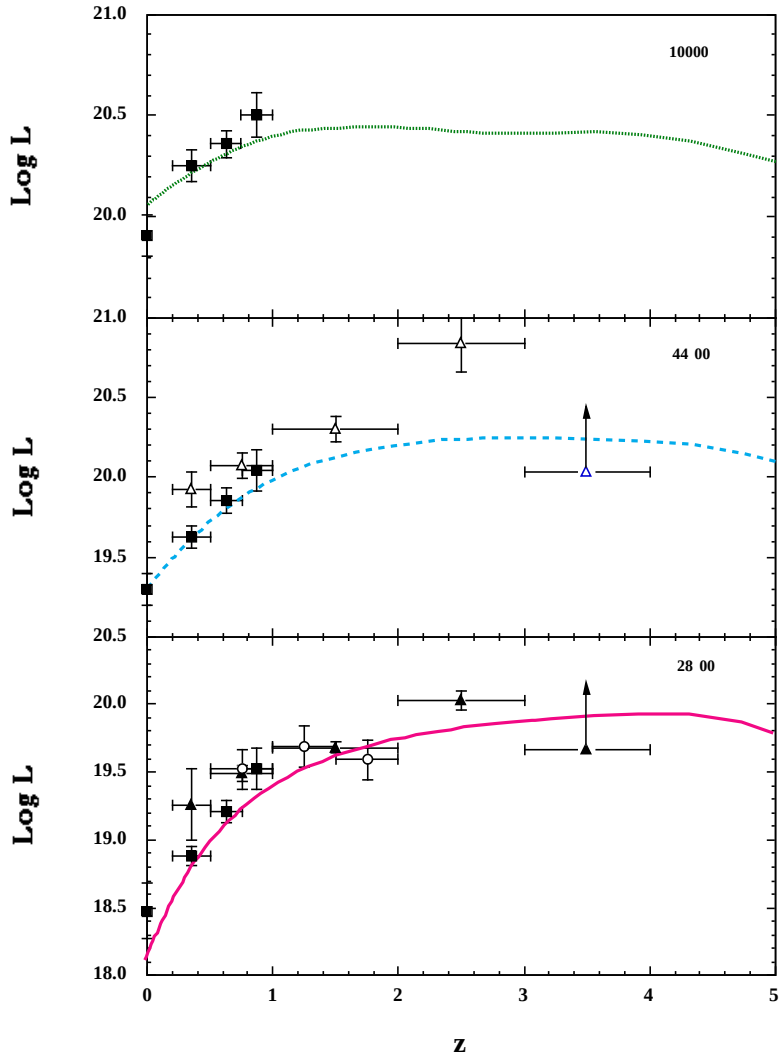

Figure 14. The tricolor luminosity densities (UV, B and IR) at $\lambda = 0.28, 0.44$ and 1.0 μm, in units of (h/.5) WHz^{-1}Mpc^{-3} as a function of redshift for a model shown in 13 which destroys significant amounts of D/H. The data are taken from [56].

that our Galaxy also has an anomalously high D/H abundance. That is we would predict in this case that the present cosmic abundance of D/H is significantly lower than the observed ISM value. If the high D/H observations [36, 37, 38] hold up, we could conclude that our Galaxy is indeed representative of the cosmic star formation history.

5. Likelihood Analyses

Monte Carlo techniques have proven to be a useful form of analysis for big bang nucleosynthesis [58, 59, 10]. An analysis of this sort was performed [2] using only ^{4}He and ^{7}Li. Two elements are sufficient for not only constraining the one parameter (η) theory of BBN, but also for testing for consistency. The procedure begins by establishing likelihood functions for the theory and observations. For example, for ^{4}He, the theoretical likelihood function takes the form

$$L_{\rm BBN}(Y, Y_{\rm BBN}) = e^{-(Y - Y_{\rm BBN}(\eta))^2/2\sigma_1^2} \tag{48}$$

where $Y_{\rm BBN}(\eta)$ is the central value for the ^{4}He mass fraction produced in the big bang as predicted by the theory at a given value of η. σ_1 is the uncertainty in that value derived from the Monte Carlo calculations [10] and is a measure of the theoretical uncertainty in the big bang calculation. Similarly one can write down an expression for the observational likelihood function. Assuming Gaussian errors, the likelihood function for the observations would take a form similar to that in (48).

A total likelihood function for each value of η is derived by convolving the theoretical and observational distributions, which for ^{4}He is given by

$$L^{^4{\rm He}}{}_{\rm total}(\eta) = \int dY\, L_{\rm BBN}\left(Y, Y_{\rm BBN}\left(\eta\right)\right) L_{\rm O}(Y, Y_{\rm O}) \tag{49}$$

An analogous calculation is performed [2] for ^{7}Li. The resulting likelihood functions from the observed abundances given in Eqs. (36) and (37) is shown in Figure 15. As one can see there is very good agreement between ^{4}He and ^{7}Li in the range of $\eta_{10} \simeq 1.5$ – 5.0. The double peaked nature of the ^{7}Li likelihood function is due to the presence of a minimum in the predicted lithium abundance. For a given observed value of ^{7}Li, there are two likely values of η.

The combined likelihood, for fitting both elements simultaneously, is given by the product of the two functions in Figure 15 and is shown in Figure 16. The 95% CL region covers the range $1.55 < \eta_{10} < 4.45$, with the two peaks occurring at $\eta_{10} = 1.9$ and 3.5. This range corresponds to values Ω_B between

$$0.006 < \Omega_B h^2 < .016 \tag{50}$$

For the lower value of $Y_p = 0.234 \pm 0.002 \pm 0.005$ as quoted in [15], the ^{4}He peak is shifted to slightly lower values of η and sits on top of the low-η peak as shown in Figure 17. (The difference in the ^{7}Li likelihood distribution is due to the assumed uncertainty in the ^{7}Li abundance which is slightly higher than that in Figure 15.) The combined likelihood in this case is shown in Figure 18. From Figure 18 it is clear that ^{4}He overlaps the

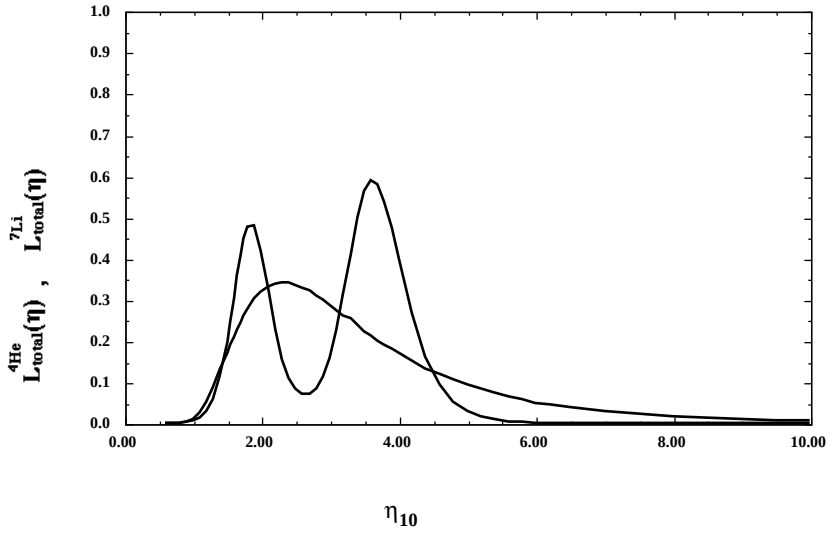

Figure 15. Likelihood distribution for each of ^{4}He and ^{7}Li, shown as a function of η. The one-peak structure of the ^{4}He curve corresponds to the monotonic increase of Y_p with η, while the two peaks for ^{7}Li arise from the minimum in the ^{7}Li abundance prediction.

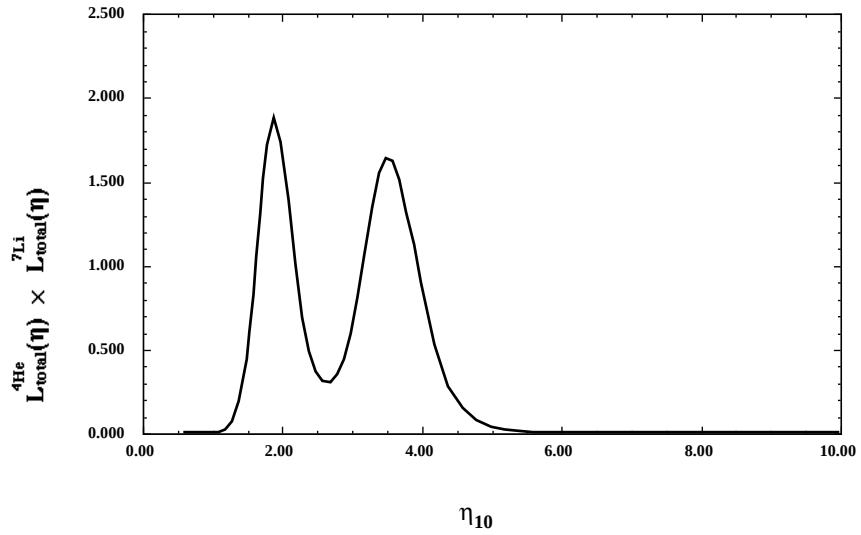

Figure 16. Combined likelihood for simultaneously fitting ^{4}He and ^{7}Li, as a function of η.

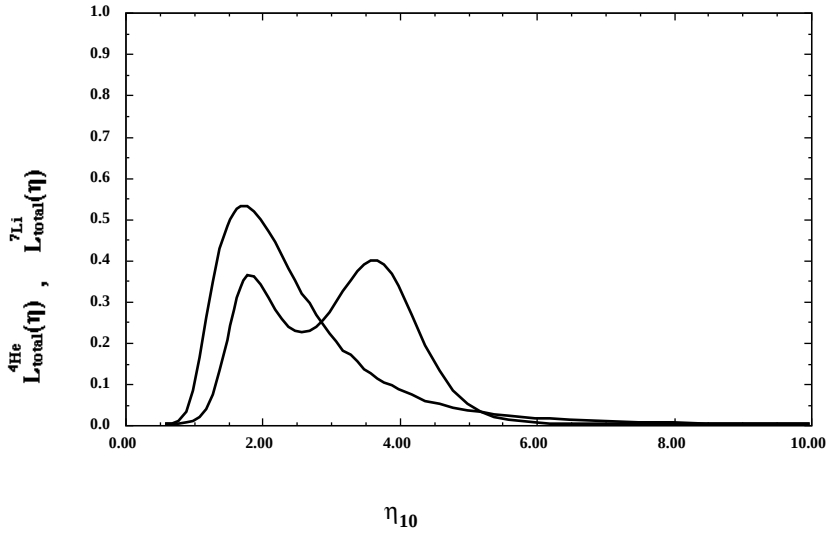

Figure 17. As in Figure 15 with a lower value of $Y_p = 0.234 \pm 0.002 \pm 0.005$.

lower (in η) ^{7}Li peak, and so one expects that there will be concordance in an allowed range of η given by the overlap region. This is what one finds in Figure 18, which does show concordance and gives a preferred value for η, $\eta_{10} = 1.8^{+2.4}_{-.4}$ corresponding to (at 95% CL) $\Omega_B h^2 = .007^{+.008}_{-.002}$.

Thus, we can conclude that the abundances of ^{4}He and ^{7}Li are consistent, and select an η_{10} range which overlaps with (at the 95% CL) the longstanding favorite range around $\eta_{10} = 3$. Furthermore, by finding concordance using only ^{4}He and ^{7}Li, we deduce that if there is problem with BBN, it must arise from D and ^{3}He and is thus tied to chemical evolution or the stellar evolution of ^{3}He. The most model-independent conclusion is that standard BBN with $N_\nu = 3$ is not in jeopardy.

It is interesting to compare the results from the likelihood function of ^{4}He and ^{7}Li with that of D/H. Since D and ^{3}He are monotonic functions of η, a prediction for η, based on ^{4}He and ^{7}Li, can be turned into a prediction for D and ^{3}He. The corresponding 95% CL ranges are D/H $= (4.3 - 25) \times 10^{-5}$ and ^{3}He/H $= (1.2 - 2.6) \times 10^{-5}$. If we did have full confidence in the measured value of D/H in quasar absorption systems, then we could perform the same statistical analysis using ^{4}He, ^{7}Li, and D. To include D/H, one would proceed in much the same way as with the other two light elements. We compute likelihood functions for the BBN predictions as in Eq. (48) and the likelihood function for the observations. These are then convolved as in Eq. (49). Using D/H $= (2.0 \pm 0.5) \times 10^{-4}$ as indicated in the high D/H systems, we can plot the three likelihood functions including

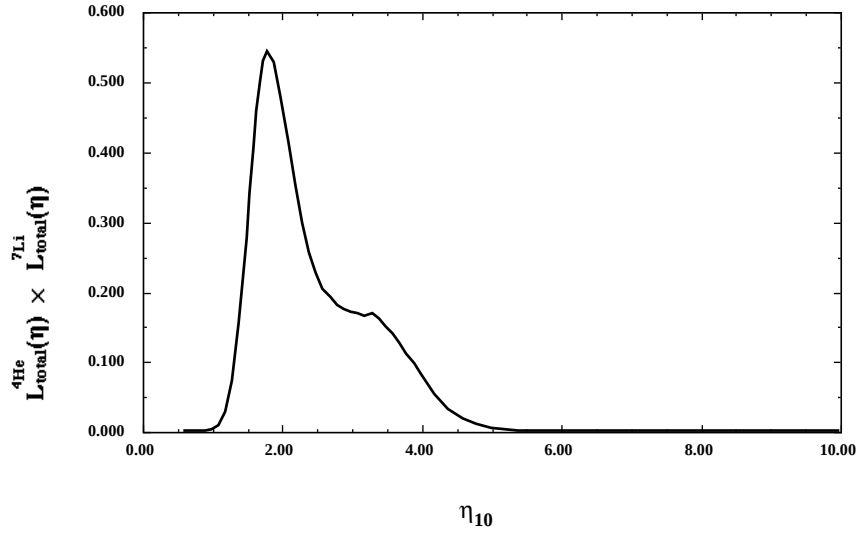

Figure 18. Combined likelihood for simultaneously fitting ^{4}He and ^{7}Li, as a function of η from from Figure 17.

$L^{\rm D}_{\rm total}(\eta)$ in Figure 19. It is indeed startling how the three peaks, for D, ^{4}He and ^{7}Li are in excellent agreement with each other. In Figure 20, the combined distribution is shown. We now have a very clean distribution and prediction for η, $\eta_{10} = 1.8^{+1.6}_{-.3}$ corresponding to $\Omega_B h^2 = .007^{+.005}_{-.001}$. The absence of any overlap with the high-η peak of the ^{7}Li distribution has considerably lowered the upper limit to η. Overall, the concordance limits in this case are dominated by the deuterium likelihood function.

If instead, we assume that the low value [40] of D/H $= (3.4 \pm 0.3) \times 10^{-5}$ is the primordial abundance, then we can again compare the likelihood distributions as in Figure 19, now substituting the low D/H value. As one can see from Figure 21, there is now hardly any overlap between the D and the ^{7}Li and ^{4}He distributions. The combined distribution shown in Figure 22 is compared with that in Figure 20. Though one can not use this likelihood analysis to prove the correctness of the high D/H measurements or the incorrectness of the low D/H measurements, the analysis clearly shows the difference in compatibility between the two values of D/H and the observational determinations of ^{4}He and ^{7}Li. To *make* the low D/H measurement compatible, one would have to argue for a shift upwards in ^{4}He to a primordial value of 0.247 (a shift by 0.009) which is not warranted at this time by the data, and a ^{7}Li depletion factor of about 2, which is close to recent upper limits to the amount of depletion [60, 28].

The implications of the resulting predictions from big bang nucleosyn-

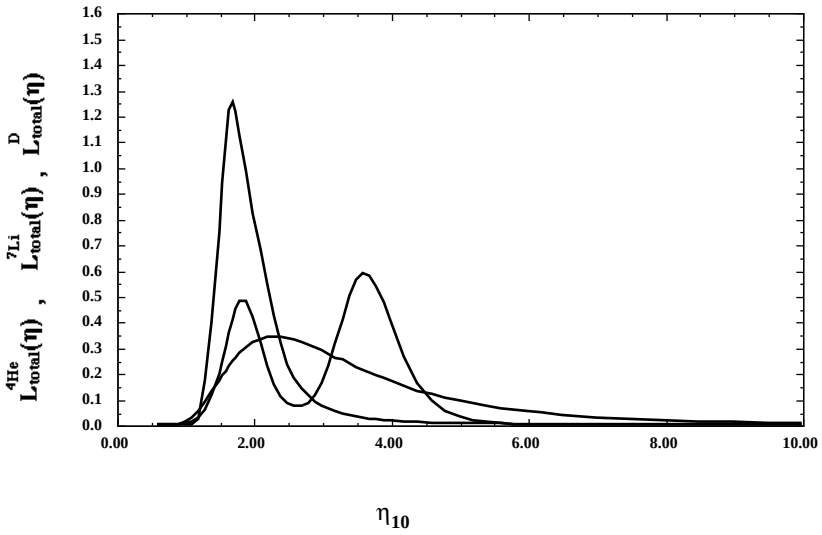

Figure 19. As in Figure 15, with the addition of the likelihood distribution for D/H assuming "high" D/H.

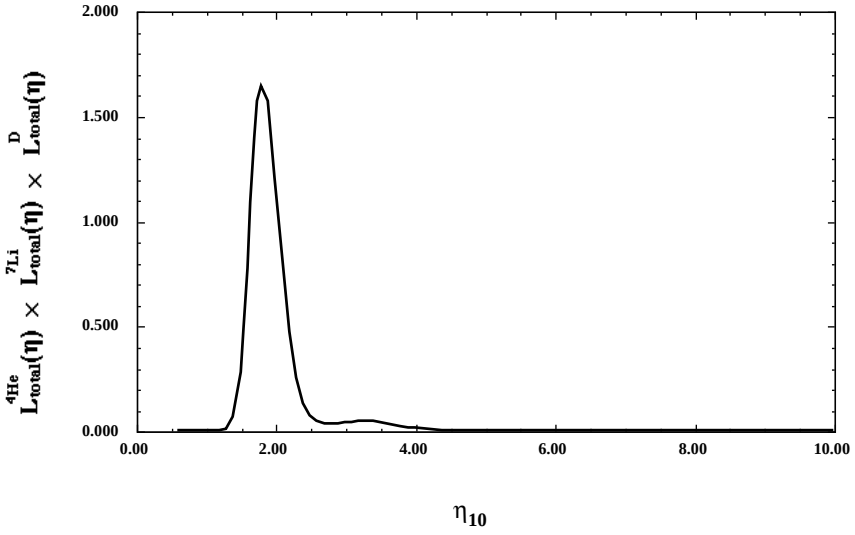

Figure 20. Combined likelihood for simultaneously fitting ^{4}He and ^{7}Li, and D as a function of η from Figure 19.

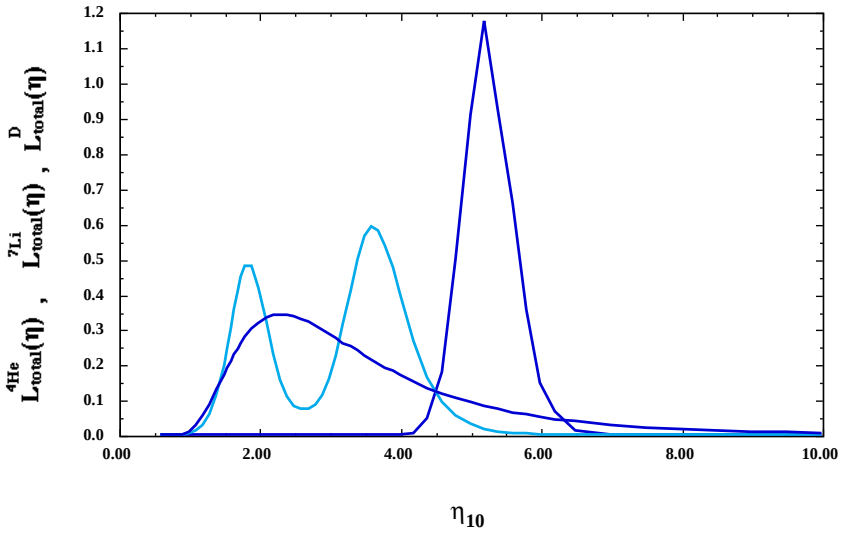

Figure 21. As in Figure 19, with the likelihood distribution for low D/H.

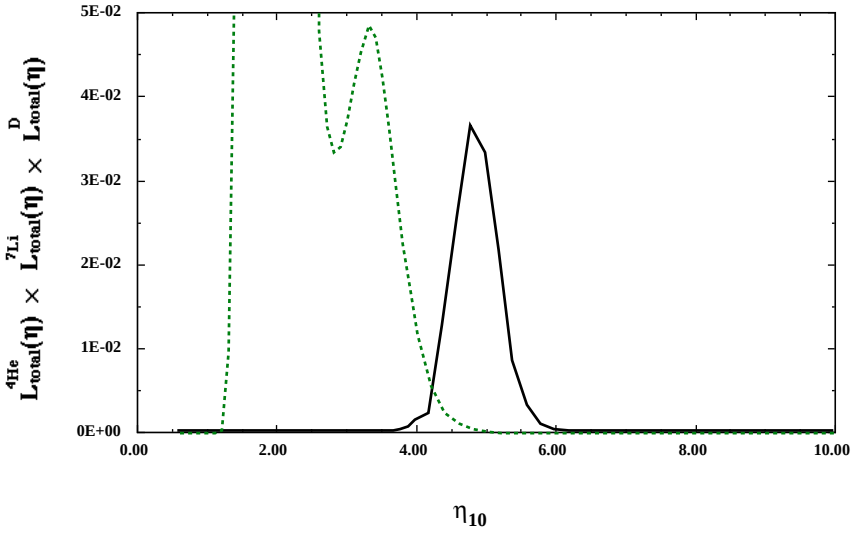

Figure 22. Combined likelihood for simultaneously fitting ^{4}He and ^{7}Li, and low D/H as a function of η. The dashed curve represents the combined distribution shown in Figure 20.

thesis on dark matter are clear. First, if $\Omega = 1$ (as predicted by inflation), and $\Omega_B \lesssim 0.1$ which is certainly a robust conclusion based on D/H, then non-baryonic dark matter is a necessity. Second, on the scale of small groups

of galaxies, which are expected to sample the dark matter in galactic halos, $\Omega \gtrsim 0.05$. This value can be compared with the best estimate for Ω_B from equation (50). The low η peak in Figure 16 corresponds to $\Omega_B h^2 = 0.007$ which for $h = 1/2$ gives $\Omega_B = 0.028$. In this event, some non-baryonic dark matter in galactic halos is required. On the other hand, the high η peak in 16 corresponds to $\Omega_B h^2 = 0.013$ which for $h = 1/2$ gives $\Omega_B = 0.051$ and may be consistent with halo densities (but only just). If we include the data from the high D/H measurements in QSO absorbers this conclusion is unchanged, only the low η peak survives, and some non-baryonic dark matter is needed in galactic halos. In contrast [61], the low D/H measurements would imply that $\Omega_B h^2 = 0.019$ allowing for the possibility that $\Omega_B \simeq 0.08$. In this case, no non-baryonic dark matter is required in galactic halos. However, I remind the reader that the low D/H value of 3.4×10^{-5} is at present only barely consistent with either the observations of ^{4}He or ^{7}Li and their interpretations as being primordial abundances.

6. Constraints from BBN

Limits on particle physics beyond the standard model are mostly sensitive to the bounds imposed on the ^{4}He abundance. As is well known, the ^{4}He abundance is predominantly determined by the neutron-to-proton ratio just prior to nucleosynthesis and is easily estimated assuming that all neutrons are incorporated into ^{4}He (see Eq. (34)). As discussed earlier, the neutron-to-proton ratio is fixed by its equilibrium value at the freeze-out of the weak interaction rates at a temperature $T_f \sim 1$ MeV modulo the occasional free neutron decay. Furthermore, freeze-out is determined by the competition between the weak interaction rates and the expansion rate of the Universe

$$G_F{}^2 T_f{}^5 \sim \Gamma_{\rm wk}(T_f) = H(T_f) \sim \sqrt{G_N N} T_f{}^2 \tag{51}$$

where N counts the total (equivalent) number of relativistic particle species. The presence of additional neutrino flavors (or any other relativistic species) at the time of nucleosynthesis increases the overall energy density of the Universe and hence the expansion rate leading to a larger value of T_f, (n/p), and ultimately Y_p. Because of the form of Eq. (51) it is clear that just as one can place limits [62] on N, any changes in the weak or gravitational coupling constants can be similarly constrained (for a recent discussion see ref. [63]). In concluding this lecture, I will discuss the current constraint on N_ν the number of particle species (in neutrino units) and the limit on the strength of new interactions, if 3 right-handed (nearly massless) neutrinos are assumed to exist.

In the past, ^{3}He (together with D) has stood out in its importance for BBN, because it provided a (relatively large) lower limit for the baryon-to-photon ratio [64], $\eta_{10} > 2.8$. This limit for a long time was seen to be

essential because it provided the only means for bounding η from below and in effect allows one to set an upper limit on the number of neutrino flavors [62], N_ν, as well as other constraints on particle physics properties. That is, the upper bound to N_ν is strongly dependent on the lower bound to η. This is easy to see: given an observed value for Y_p, for lower η, the ^{4}He abundance drops, allowing for a larger N_ν, which would raise the ^{4}He abundance back to the observed value. However, for $\eta < 4 \times 10^{-11}$, corresponding to $\Omega_B h^2 \lesssim .001 - .002$, which is not too different from galactic mass densities, there is no bound whatsoever on N_ν [65]. Of course, with the improved data on ^{7}Li, we do have lower bounds on η which exceed 10^{-10}. In fact, despite the uncertainty in the D/H abundance in quasar absorption systems, the high D/H values can certainly be regarded as an upper limit to primordial D/H, which also yield a lower limit to η.

Because, of new observations of D and ^{3}He, and the new theoretical work on chemical evolution sparked by these observations, the bound on N_ν which is tied directly to these isotopes, should be called into question. As described earlier, the limits due to ^{3}He are ultimately tied to the assumed yields of low mass stars. Using the reduced yields as depicted in Figure 13, consistent values of $\eta < 2.8$ are certainly possible. Ultimately, as I have said repeatedly, D/H measurements in quasar absorption systems may soon resolve this issue. However, the lower values of η, relax the bounds on the number of neutrino flavors.

As discussed above, the limit on N_ν comes about via the change in the expansion rate given by the Hubble parameter,

$$H^2 = \frac{8\pi G}{3}\rho = \frac{8\pi^3 G}{90}[N_{\rm SM} + \frac{7}{8}\Delta N_\nu]T^4 \tag{52}$$

when compared to the weak interaction rates. Here $N_{\rm SM}$ refers to the standard model value for N. At $T \sim 1$ MeV, $N_{\rm SM} = 43/4$. Additional degrees of freedom will lead to an increase in the freeze-out temperature eventually leading to a higher ^{4}He abundance. In fact, one can parameterize the dependence of Y on N_ν by

$$Y = 0.2262 + 0.0131(N_\nu - 3) + 0.0135 \ln \eta_{10} \tag{53}$$

in the vicinity of $\eta_{10} \sim 2$. Eq. (53) also shows the weak (log) dependence on η. However, rather than use (53) to obtain a limit, it is preferable to use the likelihood method.

Just as ^{4}He and ^{7}Li were sufficient to determine a value for η, a limit on N_ν can be obtained as well [2, 66]. The likelihood approach utilized above can be extended to include N_ν as a free parameter. Since the light element abundances can be computed as functions of both η and N_ν, the likelihood

function can be defined by [66]

$$L_{\rm BBN}(Y, Y_{\rm BBN}) = e^{-(Y - Y_{\rm BBN}(\eta, N_\nu))^2/2\sigma_1^2} \tag{54}$$

and

$$L^{^4{\rm He}}{}_{\rm total}(\eta, N_\nu) = \int dY\, L_{\rm BBN}\left(Y, Y_{\rm BBN}\left(\eta, N_\nu\right)\right) L_{\rm O}(Y, Y_{\rm O}) \tag{55}$$

Again, similar expressions are needed for ^{7}Li and D. A three-dimensional view of the combined likelihood functions [66] is shown in Figure 23 which is based on the slightly lower value of Y_p as used in Figure 17. For updated (but similar) results see [67]. In this case the high and low η maxima of Figure 18, show up as peaks in the $L - \eta - N_\nu$ space (L_{47} when D/H is neglected and L_{247} when high D/H is included). The peaks of the distribution as well as the allowed ranges of η and N_ν are more easily discerned in the contour plot of Figure 24 which shows the 50%, 68% and 95% confidence level contours in the two likelihood functions. The crosses show the location of the peaks of the likelihood functions. L_{47} peaks at $N_\nu = 3.0$, $\eta_{10} = 1.8$ (in agreement with our previous results [2]) and at $N_\nu = 2.3$, $\eta_{10} = 3.6$. The 95% confidence level allows the following ranges in η and N_ν

$$1.6 \leq N_\nu \leq 4.0 \qquad\qquad 1.3 \leq \eta_{10} \leq 5.0 \tag{56}$$

Note however that the ranges in η and N_ν are strongly correlated as is evident in Figure 24. Since the deuterium likelihood function picks out a small range of values of η, largely independent of N_ν, its effect on L_{247} is to eliminate one of the two peaks in L_{47}. L_{247} also peaks at $N_\nu = 3.0$, $\eta_{10} = 1.8$. In this case the 95% contour gives the ranges

$$2.0 \leq N_\nu \leq 4.1 \qquad\qquad 1.4 \leq \eta_{10} \leq 2.6 \tag{57}$$

Finally, in Figure 25, the resulting 95 % CL upper limit to N_ν is shown as a function of Y_P for several different choices for the primordial value of ^{7}Li/H [67].

One should recall that the limit derived above is not meant for neutrinos in the strictest sense. That is, the limit is only useful when applied to additional particle degrees of freedom which necessarily do not couple to the Z^o. For very weakly interacting particles, one must take into account the reduced abundance of these particles at the time of nucleosynthesis[68]. As discussed in the first lecture, the number of neutrinos today is reduced relative to the number of photons by $(T_\nu/T_\gamma)^3 = 4/11$. For some new particle, χ, which decoupled at $T_d > 1$ MeV, the same argument based on the conservation of entropy tells us that

$$(\frac{T_\chi}{T_\gamma})^3 = \frac{43}{4N(T_d)} \tag{58}$$

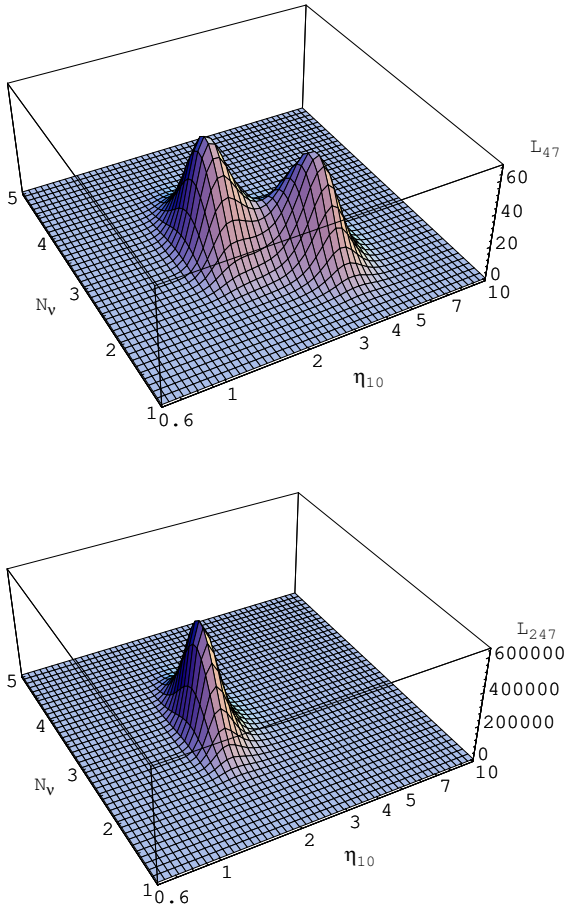

Figure 23. The combined two-dimensional likelihood functions for simultaneously fitting ^{4}He and ^{7}Li in the top panel, and including D in the lower one as functions of both η and N_ν.

Thus we can translate the bound on N_ν, which is really a bound on the additional energy density at nucleosynthesis

$$\Delta\rho = \frac{\pi^2}{30}\left[\sum g_B(\frac{T_B}{T})^4 + \frac{7}{8}\sum g_F(\frac{T_F}{T})^4\right]T^4 \qquad (59)$$

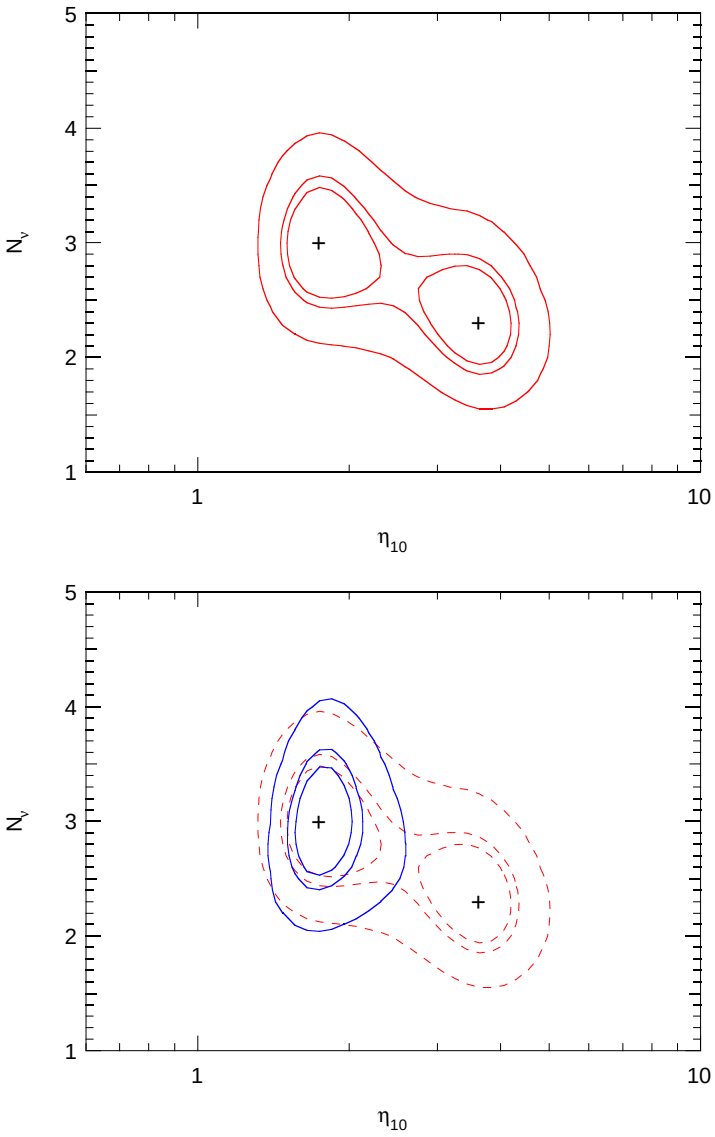

Figure 24. The top panel shows contours in the combined likelihood function for ^{4}He and ^{7}Li. The contours represent 50% (innermost), 68% and 95% (outermost) confidence levels. The crosses mark the points of maximum likelihood. Also shown is the equivalent result when D is included.

for additional boson states with g_B degrees of freedom and fermion states with g_F degrees of freedom. At nucleosynthesis $T = T_\nu = T_\gamma$ and the limit

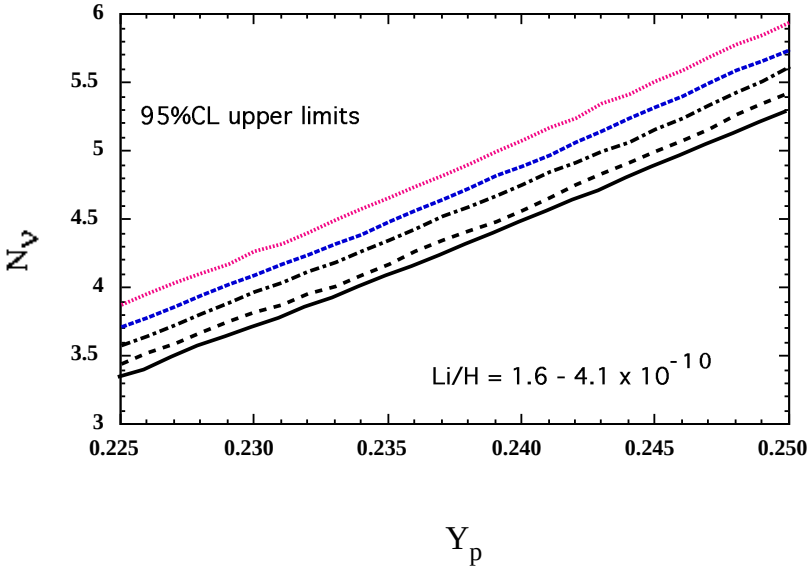

Figure 25. The 95 % CL upper limit to N_ν as a function of Y_p for $(\mathrm{Li/H})_p$ = 1.6, 2.0, 2.6, 3.2, and 4.1 $\times 10^{-10}$.

$N_\nu < 4$ becomes

$$\frac{8}{7}\sum \frac{g_B}{2}(\frac{T_B}{T_\nu})^4 + \sum \frac{g_F}{2}(\frac{T_F}{T})^4 < 1 \tag{60}$$

Such a limit would allow a single additional scalar degree of freedom (which counts as $\frac{4}{7}$) such as a majoron. On the other hand, in models with right-handed interactions, and three right-handed neutrinos, the constraint is severe. The right-handed states must have decoupled early enough to ensure $(T_{\nu_R}/T_{\nu_L})^4 < 1/3$. The temperature of a decoupled state is easily determined from (58). Three right-handed neutrinos would require $N(T_d) \gtrsim 25$, which from Figure 1 implies that $T_d > 140$ MeV, conservatively assuming a QCD transition temperature of 150 MeV. If right-handed interactions are mediated by additional gauge interactions, associated with some scale $M_{Z'}$, and if we assume that the right handed interactions scale as $M_{Z'}^4$ with a standard model-like coupling, then the decoupling temperature of the right handed interactions is related to $M_{Z'}$ by

$$(\frac{T_{dR}}{T_{dL}})^3 \sim (\frac{M_{Z'}}{M_Z})^4 \tag{61}$$

which for $T_{dL} \sim 3$ MeV (a more accurate value that the 1 MeV estimate) and $T_{dL} \gtrsim 140$ MeV, we find that the associated mass scale becomes $M_{Z'} \gtrsim$

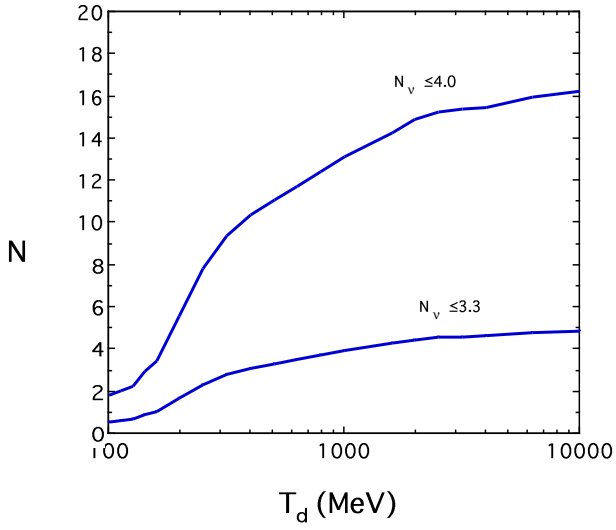

Figure 26. Limits on neutrino-like degrees of freedom.

1.6 TeV! In general this constraint is very sensitive to the BBN limit on N_ν. In Figure 26, the allowed number of neutrino degrees of freedom are shown as a function of their decoupling temperature for the case of $N_\nu < 4$ and $N_\nu < 3.3$, shown for comparison.

7. Summary

To summarize on the subject of big bang nucleosynthesis, I would assert that one can conclude that the present data on the abundances of the light element isotopes are consistent with the standard model of big bang nucleosynthesis. Using the the isotopes with the best data, ^{4}He and ^{7}Li, it is possible to constrain the theory and obtain a best set of values for the baryon-to-photon ratio of η_{10} and the corresponding value for $\Omega_B h^2$

$$\begin{array}{ccccccc} 1.55 & < & \eta_{10} & < & 4.45 & \quad & 95\%\text{CL} \\ .006 & < & \Omega_B h^2 & < & .016 & \quad & 95\%\text{CL} \end{array} \tag{62}$$

For $0.4 < h < 1$, we have a range $.006 < \Omega_B < .10$. This is a rather low value for the baryon density and would suggest that much of the galactic dark matter is non-baryonic [69]. These predictions are in addition consistent with recent observations of D/H in quasar absorption systems which show a high value. Difficulty remains however, in matching the solar ^{3}He abundance, suggesting a problem with our current understanding of galactic chemical evolution or the stellar evolution of low mass stars as they pertain to ^{3}He.

References

1. G.F.R. Ellis, these proceedings.
2. B.D. Fields and K.A. Olive, *Phys. Lett.* **B368** (1996) 103; B.D. Fields, K. Kainulainen, D. Thomas, and K.A. Olive, *New Astronomy* **1** (1996) 77.
3. G.F. Smoot and D. Scott, *Eur. Phys. J.* **C3** (1998) 127.
4. G. Gamow, *Phys. Rev.* **74** (1948) 505; G. Gamow, *Nature* **162** (1948) 680; R.A. Alpher and R.C. Herman, *Nature* **162** (1948) 774; R.A. Alpher and R.C. Herman, *Phys. Rev.* **75** (1949) 1089.
5. E.M. Burbidge, G.R. Burbidge, W.A. Fowler, and F. Hoyle, *Rev. Mod. Phys.* **29** (1957) 547.
6. H. Reeves, J. Audouze, W.A. Fowler, and D.N. Schramm, *Ap.J.* **179** (1973) 909.
7. C. Hayashi, *Prog. Theor. Phys.* **5** (1950) 224; R.A. Alpher, J.W. Follin Jr., R.C. Herman, *Phys. Rev.* **92** (1953) 1347; Ya. B. Zel'dovich, *Sov. Phys. Usp.* **6** (1963) 475; F. Hoyle and R.J. Taylor, *Nature* **203** (1964) 1108; P.J.E. Peebles, *Ap.J.* **146** (1966) 542; R.A. Wagoner, W.A. Fowler, and F. Hoyle, *Ap.J.* **148** (1967) 3; R.A. Wagoner, *Ap.J.* **179** (1973) 343.
8. D. Thomas, D. Schramm, K.A. Olive, and B. Fields, *Ap.J.* **406** (1993) 569.
9. Review of Particle Properties, *Phys. Rev.* **54** (1996) 1.
10. N. Hata, R.J. Scherrer, G. Steigman, D. Thomas, and T.P. Walker, *Ap.J.* **458** (1996) 637.
11. B.E.J. Pagel, E.A. Simonson, R.J. Terlevich and M. Edmunds, *MNRAS* **255** (1992) 325.
12. E. Skillman and R.C. Kennicutt, *Ap.J.* **411** (1993) 655; E. Skillman, R.J. Terlevich, R.C. Kennicutt, D.R. Garnett, and E. Terlevich, *Ap.J.* **431** (1994) 172.
13. Y.I. Izotov, T.X. Thuan, and V.A. Lipovetsky, *Ap.J.* **435** (1994) 647; *Ap.J.S.* **108** (1997) 1.
14. K.A. Olive and G. Steigman, *Ap.J. Supp.* **97** (1995) 49.
15. K.A. Olive, E. Skillman, and G. Steigman, *Ap.J.* **483** (1997) 788.
16. K.A. Olive and S.T. Scully, *IJMPA* **11** (1995) 409.
17. C.J. Hogan, K.A. Olive, and S.T. Scully, *Ap.J.* **489** (1997) L119.
18. Y.I. Izotov, and T.X. Thuan, *Ap.J.* **500** (1998) 188.
19. B.D. Fields and K.A. Olive, *Ap.J.* **506** (1998) 177
20. F. Spite, and M. Spite, *A.A.* **115** (1982) 357; M. Spite, J.P. Maillard, and F. Spite, *A.A.* **141** (1984) 56; F. Spite, and M. Spite, *A.A.* **163** (1986) 140; L.M. Hobbs, and D.K. Duncan, *Ap.J.* **317** (1987) 796; R. Rebolo, P. Molaro, J.E. and Beckman, *A.A.* **192** (1988) 192; M. Spite, F. Spite, R.C. Peterson, and F.H. Chaffee Jr., *A.A.* **172** (1987) L9; R. Rebolo, J.E. Beckman, and P. Molaro, *A.A.* **172** (1987) L17; L.M. Hobbs, and C. Pilachowski, *Ap.J.* **326** (1988) L23; L.M. Hobbs, and J.A. Thorburn, *Ap.J.* **375** (1991) 116; J.A. Thorburn, *Ap.J.* **399** (1992) L83; C.A. Pilachowski, C. Sneden,and J. Booth, *Ap.J.* **407** (1993) 699; L. Hobbs, and J. Thorburn, *Ap.J.* **428** (1994) L25; J.A. Thorburn, and T.C. Beers, *Ap.J.* **404** (1993) L13; F. Spite, and M. Spite, *A.A.* **279** (1993) L9. J.E. Norris, S.G. Ryan, and G.S. Stringfellow, *Ap.J.* **423** (1994) 386.
21. P. Molaro, F. Primas, and P. Bonifacio, *A.A.* **295** (1995) L47; P. Bonifacio and P. Molaro, *MNRAS* **285** (1997) 847.
22. J. Thorburn, *Ap.J.* **421** (1994) 318.
23. K. Fuhrmann, M. Axer, and T. Gehren, *A. A.* **285** (1994) 585.
24. A. Alonso, S. Arribas, and C. Martinez-Roger, C. *A. A. Supp.* **117** (1996) 227.
25. C.P. Deliyannis, P. Demarque, and S.D. Kawaler, *Ap.J.Supp.* **73** (1990) 21.
26. V.V. Smith, D.L. Lambert, and P.E. Nissen, *Ap.J.* **408** (1992) 262; *Ap.J.* (1998) in press; L. Hobbs, and J. Thorburn, *Ap.J.* **428** (1994) L25; M. Spite et al. *A.A.* (1998) submitted.
27. G. Steigman, B. Fields, K.A. Olive, D.N. Schramm, and T.P. Walker, *Ap.J.* **415** (1993) L35; M. Lemoine, D.N. Schramm, J.W. Truran, and C.J. Copi, *Ap.J.* **478**

(1997) 554.
28. M.H. Pinsonneault, T.P. Walker, G. Steigman, and V.K. Naranyanan, *Ap.J.* (1998) submitted.
29. B.D.Fields and K.A. Olive, *New Astronomy*, astro-ph/9811183, in press; E. Vangioni-Flam, et al. *New Astronomy*, in press.
30. T.P. Walker, G. Steigman, D.N. Schramm, K.A. Olive and B. Fields, *Ap.J.* **413** (1993) 562; K.A. Olive, and D.N. Schramm, *Nature* **360** (1993) 439.
31. J.L. Linsky, et al., *Ap.J.* **402** (1993) 694; J.L. Linsky, et al.,*Ap.J.* **451** (1995) 335.
32. S.T. Scully, M. Cassé, K.A. Olive, D.N. Schramm, J.W. Truran, and E. Vangioni-Flam, *Ap.J.* **462** (1996) 960.
33. J. Geiss, in *Origin and Evolution of the Elements*, eds. N. Prantzos, E. Vangioni-Flam, and M. Cassé (Cambridge: Cambridge University Press, 1993), p. 89.
34. H.B. Niemann, et al. *Science* **272** (1996) 846.
35. C. Copi, K.A. Olive, and D.N. Schramm, *Proc. Nat. Ac. Sci.* **95** (1998) 2758, astro-ph/9606156.
36. R.F. Carswell, M. Rauch, R.J. Weymann, A.J. Cooke, and J.K. Webb, *MNRAS* **268** (1994) L1; A. Songaila, L.L. Cowie, C. Hogan, and M. Rugers, *Nature* **368** (1994) 599.
37. M. Rugers and C.J. Hogan, *A.J.* **111** (1996) 2135; R.F. Carswell, et al. *MNRAS* **278** (1996) 518; E.J. Wampler, et al., *A.A. 316* (1996) 33.
38. J.K. Webb, R.F. Carswell, K.M. Lanzetta, R. Ferlet, M. Lemoine, A. Vidal-Madjar, and D.V. Bowen, *Nature* **388** (1997) 250; D. Tytler et al., astro-ph/9810217 (1998).
39. D. Tytler, X.-M. Fan, and S. Burles, *Nature* **381** (1996) 207; S. Burles and D. Tytler, *Ap.J.* **460** (1996) 584.
40. S. Burles and D. Tytler, *Ap.J.* **499** (1998) 699; and astro-ph/9712109.
41. A. Songaila, E.J. Wampler, and L.L. Cowie, *Nature* **385** (1997) 137.
42. D.S. Balser, T.M. Bania, C.J. Brockway, R.T. Rood, and T.L. Wilson, *Ap.J.* **430** (1994) 667; T.M. Bania, D.S. Balser, R.T. Rood, T.L. Wilson, and T.J. Wilson, *Ap.J.S.* **113** (1997) 353.
43. K.A. Olive, R.T. Rood, D.N. Schramm, J.W. Truran, and E. Vangioni-Flam, *Ap.J.* **444** (1995) 680.
44. G. Gloeckler, and J. Geiss, *Nature* **381** (1996) 210.
45. R.T. Rood, T.M. Bania, and T.L. Wilson, Nature **355** (1992) 618; R.T. Rood, T.M. Bania, T.L. Wilson, and D.S. Balser, 1995, in *the Light Element Abundances, Proceedings of the ESO/EIPC Workshop*, ed. P. Crane, (Berlin:Springer), p. 201; D.S. Balser, T.M. Bania, R.T. Rood, T.L. Wilson, *Ap.J.* **483** (1997) 320.
46. B.M. Tinsley, *Fund. Cosmic Phys.,* **5** (1980) 287.
47. I. Iben, and J.W. Truran, *Ap.J.* **220** (1978) 980.
48. D. Galli, F. Palla, F. Ferrini, and U. Penco, Ap.J. **443** (1995) 536; D. Dearborn, G. Steigman, and M. Tosi, *Ap.J.* **465** (1996) 887.
49. S. Scully, M. Cassé, K.A. Olive, and E. Vangioni-Flam, *Ap.J.* **476** (1997) 521.
50. C. Charbonnel, *A. A.* **282** (1994) 811; C. Charbonnel, *Ap.J.* **453** (1995) L41; C.J. Hogan, *Ap.J.* **441** (1995) L17; G.J. Wasserburg, A.I. Boothroyd, andI.-J. Sackmann, *Ap.J.* **447** (1995) L37; A. Weiss, J. Wagenhuber, and P. Denissenkov, *A.A.* **313** (1996) 581.
51. A.I. Boothroyd, A.I. and R.A. Malaney, astro-ph/9512133.
52. K.A. Olive, D.N. Schramm, S. Scully, and J.W. Truran, *Ap.J.* **479** (1997) 752.
53. D. Galli, L. Stanghellini, M. Tosi, and F. Palla *Ap.J.* **477** (1997) 218.
54. R. Mushotzky, et al., *Ap.J.* **466** (1996) 686
55. M. Loewenstein and R. Mushotzky, *Ap.J.* **466** (1996) 695.
56. S.J. Lilly, O. Le Fevre, F. Hammer, and D. Crampton, *ApJ* **460** (1996) L1; P. Madau, H.C. Ferguson, M.E. Dickenson, M. Giavalisco, C.C. Steidel, and A. Fruchter, *MNRAS* **283** (1996) 1388; A.J. Connolly, A.S. Szalay, M. Dickenson, M.U. SubbaRao, and R.J. Brunner, *ApJ* **486** (1997) L11; M.J. Sawicki, H. Lin, and H.K.C. Yee, *A.J.* **113** (1997) 1.
57. M. Cassé, K.A. Olive, E. Vangioni-Flam, and J. Audouze, *New Astronomy* **3** (1998)

259.
58. L.M. Krauss and P. Romanelli, *Ap.J.* **358** (1990) 47; L.M. Krauss and P.J. Kernan, *Phys. Lett.* **B347** (1995) 347; M. Smith, L. Kawano, and R.A. Malaney, *Ap.J. Supp.* **85** (1993) 219.
59. P.J. Kernan and L.M. Krauss, *Phys. Rev. Lett.* **72** (1994) 3309.
60. S. Vauclair and C. Charbonnel, *A.A.* **295** (1995) 715.
61. C.Y. Cardall and G.M. Fuller, *Ap.J.* **472** (1996) 435; N. Hata, G. Steigman, S. Bludman, and P. Langacker, *Phys.Rev.* **D55** (1997) 540.
62. G. Steigman, D.N. Schramm, and J. Gunn, *Phys. Lett.* **B66** (1977) 202.
63. B.A. Campbell and K.A. Olive, *Phys. Lett.* **B345** (1995) 429.
64. J. Yang, M.S. Turner, G. Steigman, D.N. Schramm, and K.A. Olive, *Ap.J.* **281** (1984) 493.
65. K.A. Olive, D.N. Schramm, G. Steigman, M.S. Turner, and J. Yang, *Ap.J.* **246** (1981) 557.
66. K.A. Olive and D. Thomas, *Astro. Part. Phys.* **7** (1997) 27.
67. K.A. Olive and D. Thomas, hep-ph/9811444.
68. G. Steigman, K.A. Olive, and D.N. Schramm, *Phys. Rev. Lett.* **43** (1979) 239; K.A. Olive, D.N. Schramm, and G. Steigman, *Nucl. Phys.* **B180** (1981) 497.
69. E. Vangioni-Flam and M. Cassé, Ap.J. **441** (1995) 471.